Supplementary Information (SI) for Journal of Materials Chemistry A.
This journal is © The Royal Society of Chemistry 2026

Supporting Information

Molecular Packing Modulated Photocatalytic Degradation using Cocrystal Catalysts

Table of Contents

1. Reagents and materials

Octafluoronaphthalene (OFN, CAS: 313-72-4, 98 %) was purchased from TCI Co.; Phenanthrene (Phe, CAS: 85-01-8, 97 %), Pyrene (Py, CAS: 129-00-0, 98 %) and Coronene (Cor, CAS: 191-07-1, 95 %) were purchased from Tianjin Heowns OPDE Technologies, LLC; Dichloromethane (CH_2Cl_2, HPLC) and L-Ascorbic acid (AA, CAS:50-81-7, 99 %) were purchased from Shanghai Macklin Biochemical Co. Propanone (C_3H_6O, AR) and Ethylenediamine($C_2H_8N_2$, CAS: 107-15-3, AR) were purchased from Tianjin Jiangtian Chemical Co.; Methanol (CH_3OH, HPLC), Tetrahydrofuran (C_4H_8O, HPLC) and Isopropanol (C_3H_8O, HPLC) were purchased from Meryer (Shanghai) Biochemical Technology Co. All the reagents were used directly without further purification.

2. Synthesis of cocrystal powders

OFN-based cocrystal photocatalyst powders were prepared by liquid-assisted grinding. OFN (1 mmol) and Phe (1 mmol) were placed in an agate mortar, and 200 μL of dichloromethane was then added. The mixture was ground and homogenized for 2 minutes. Subsequently, another 100 μL of dichloromethane was added, and grinding was continued for an additional minute, ultimately producing a significant amount of cocrystal powder. Similarly, the OFN-Py cocrystal powders were prepared using acetone as the solvent, while the OFN-Cor cocrystal powders utilized tetrahydrofuran (THF), all following the same preparation procedure.

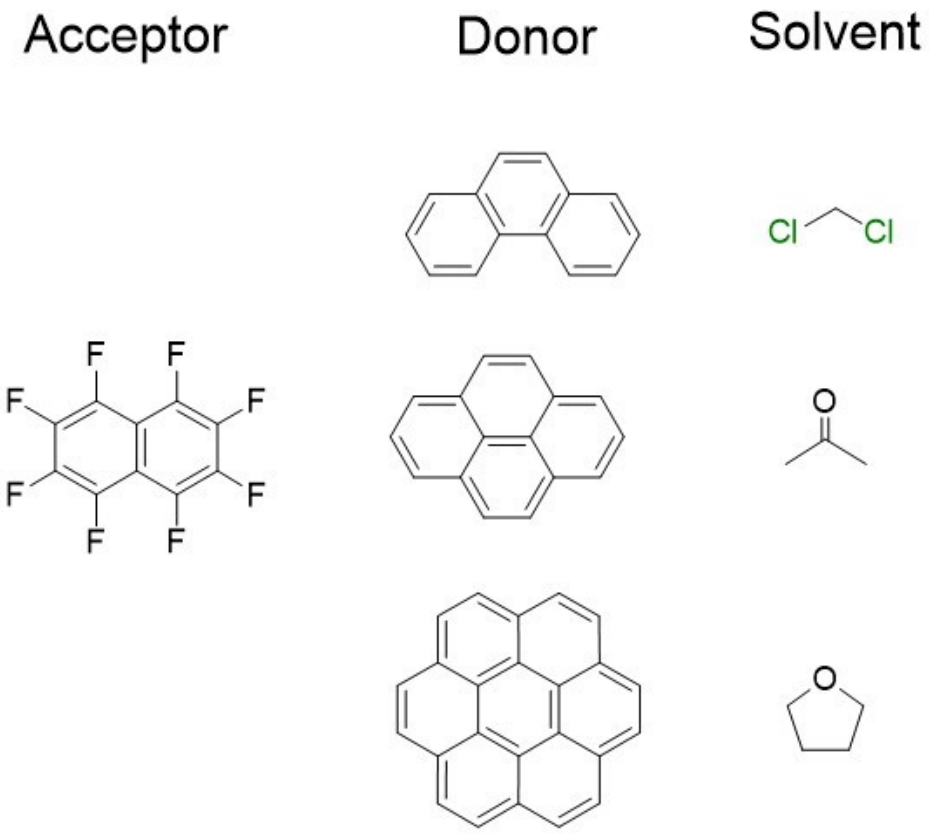

Figure S1. The chemical structures of donor, acceptor and solvent.

3. Optical images

Micro-nano cocrystals were prepared using the droplet-casting method. Specifically, THF solutions of OFN-Phe (1 mg·mL^{-1}), OFN-Py (0.5 mg·mL^{-1}), and OFN-Cor (0.5 mg·mL^{-1}) were individually drop-cast (150 μL each) onto pre-cleaned glass substrates. After solvent evaporation under ambient conditions overnight, highly crystalline needle-like cocrystals were obtained. The resulting crystals were imaged using optical microscopy to obtain representative morphologies.

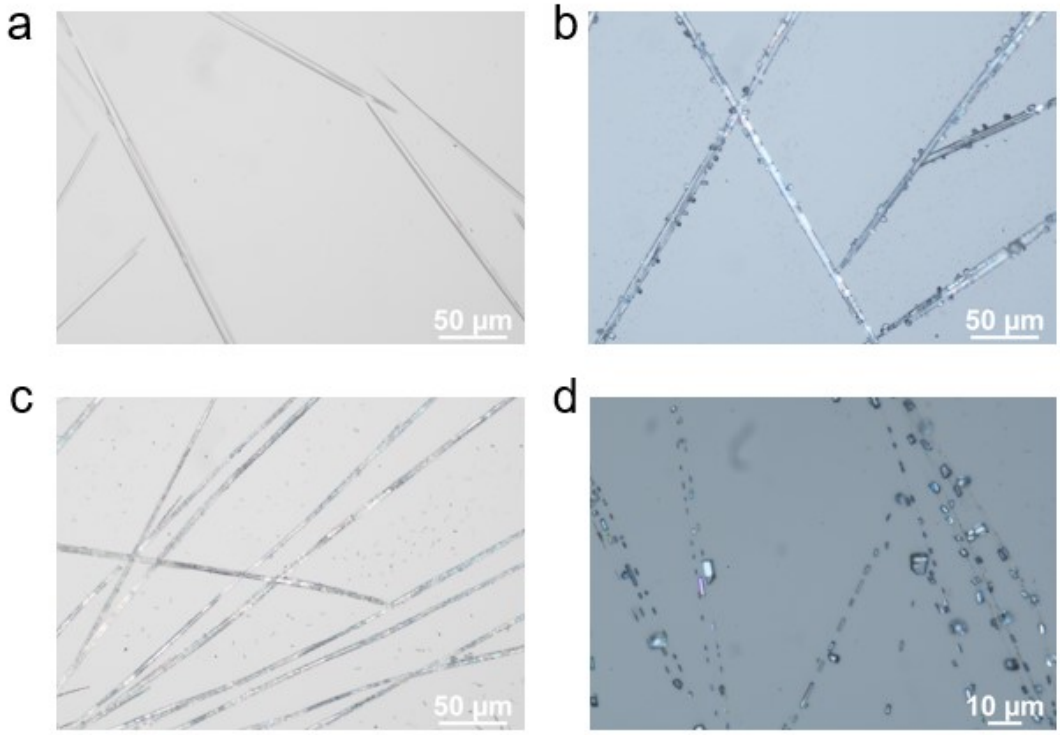

Figure S2. Optical images of micro-nano crystals. (a) OFN-Phe, (b, d) OFN-Py and (c) OFN-Cor.

4. Scanning Electron Microscopy (SEM)

A homogeneous aqueous dispersion (1.25 mg·mL^{-1}) was prepared by ultrasonication. An appropriate volume of the dispersion was then drop-cast onto a Si/SiO_2 substrate and dried naturally at room temperature for morphological characterization of the material in aqueous media. Field-emission scanning electron microscopy (FESEM, HITACHI UHR SU8000; provided by the Tianjin Key Laboratory of Molecular Optoelectronic Sciences) was performed under an accelerating voltage of 10 kV to visualize the surface morphology. As shown in Figure S3, SEM characterization confirms that the morphologies of both cocrystals remain essentially unchanged before and after the photocatalytic reactions. The absence of obvious surface erosion or particle fragmentation suggests that the cocrystals maintain good structural stability during photocatalytic operation.

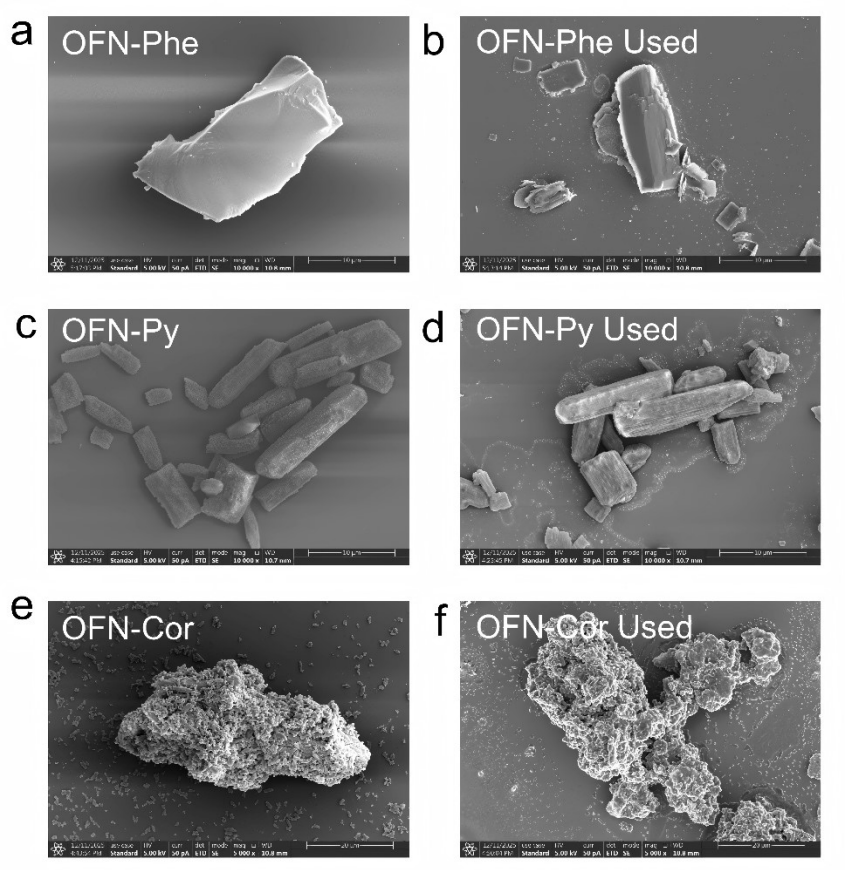

Figure S3. Morphology of cocrystals before and after photocatalytic reaction. (a, b) OFN-Phe, (c, d) OFN-Py and (e, f) OFN-Cor.

5. Single Crystal X-ray Diffraction (SXRD)

Single crystal growth: Large single crystals suitable for SXRD analysis were obtained via a solution evaporation crystallization method. Specifically, equimolar amounts of OFN (0.03 mmol) and Phe (0.03 mmol) were dissolved in 5 mL of THF to afford a homogeneous solution. The solution was left undisturbed at room temperature to allow slow solvent evaporation. As the concentration gradually increased to a supersaturated state, crystal nucleation and subsequent slow growth were induced. After two weeks of controlled evaporation, centimeter-scale cocrystals were successfully harvested.

Data collection and processing: Single-crystal X-ray diffraction (SXRD) data were collected on a Rigaku XtaLAB P200 instrument (School of Chemistry, Nankai University) using Cu Kα radiation (λ = 1.54184 Å). A suitable single crystal was selected and mounted on the HyPix-Arc 150 detector, which is part of the ROD-type SynergyCustom DW system. During data collection, the crystal was maintained at a temperature of 100.00(10) K. Using Olex 2[1] the structure was solved with the ShelXT structure solution program using Intrinsic Phasing and refined with the XL refinement package using Least Squares minimization.

The following formula is used to calculate the distance between molecules[2]:

$$l = \frac{L_D + L_A}{4}$$

l: the distance between the donor and the acceptor in the cocrystal molecule;

L_D: the distance between the two donors in the cocrystal molecule;

L_A: the distance between the two acceptors in the cocrystal molecule.

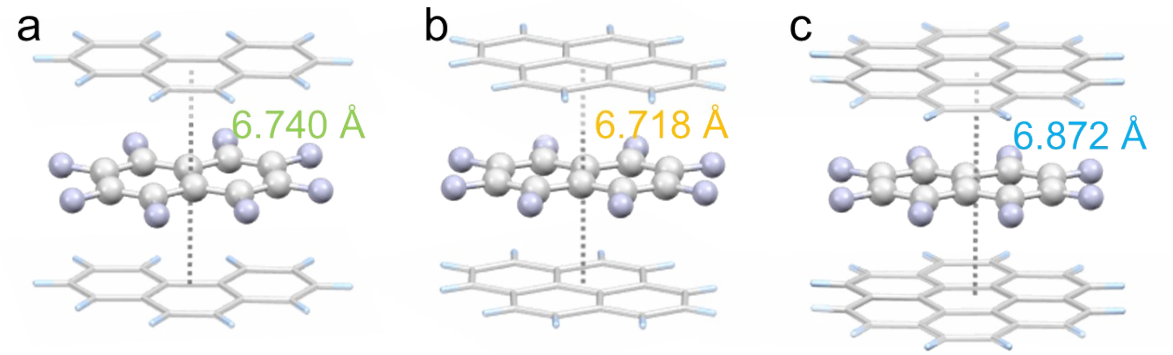

Figure S4. Distance between [D···A···D] repeating unit. (a) OFN-Phe, (b) OFN-Py and (c) OFN-Cor.

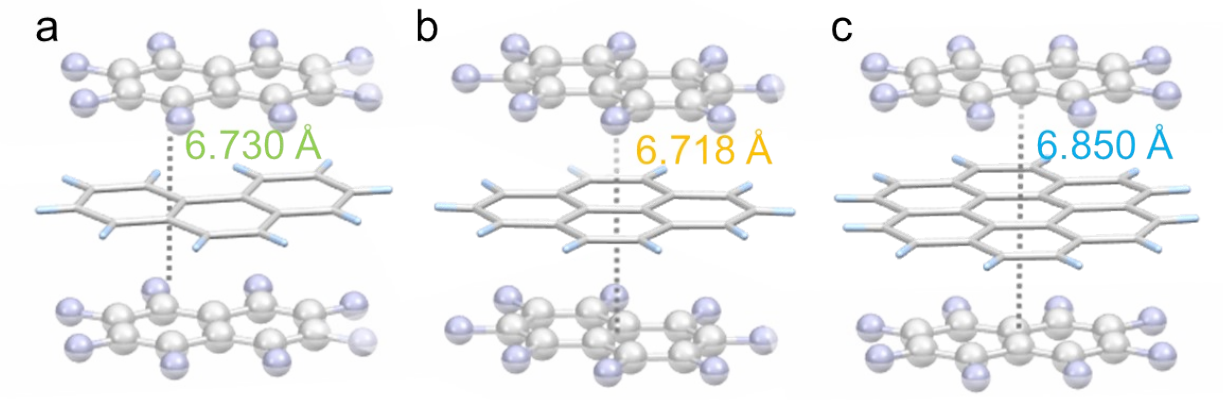

Figure S5. Distance between [A···D···A] repeating unit. (a) OFN-Phe, (b) OFN-Py and (c) OFN-Cor.

As for OFN-Phe, the distance between donor and acceptor is

$$\frac{6.740 + 6.730}{4} = 3.3675 \text{ Å}.$$

As for OFN-Py, the distance between donor and acceptor is

$$\frac{6.718 + 6.718}{4} = 3.3590 \text{ Å}.$$

As for OFN-Cor, the distance between donor and acceptor is

$$\frac{6.872 + 6.850}{4} = 3.4305 \text{ Å}.$$

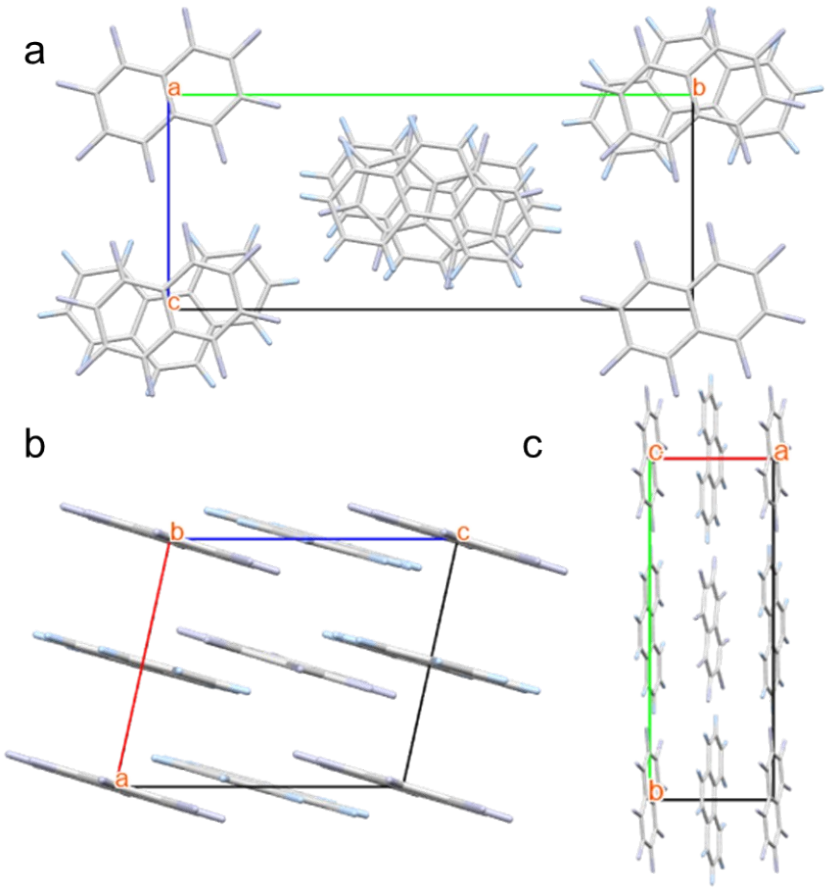

Figure S6. Cell structure of OFN-Phe. (a) From the a-axis, (b) from the b-axis, and (c) from the c-axis.

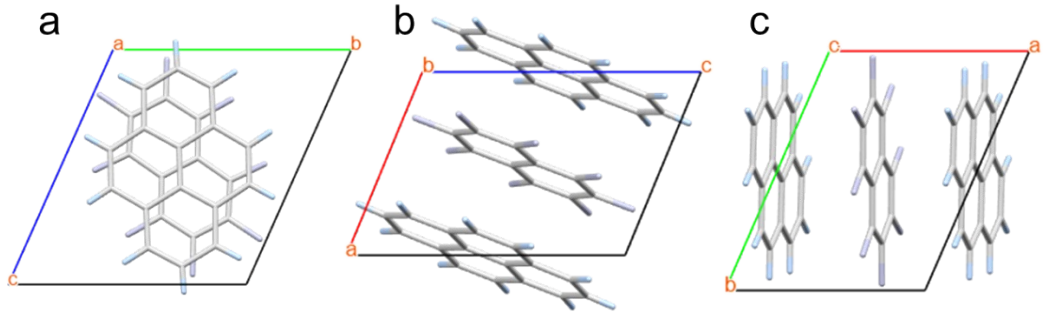

Figure S7. Cell structure of OFN-Py. (a) From the a-axis, (b) from the b-axis, and (c) from the c-axis.

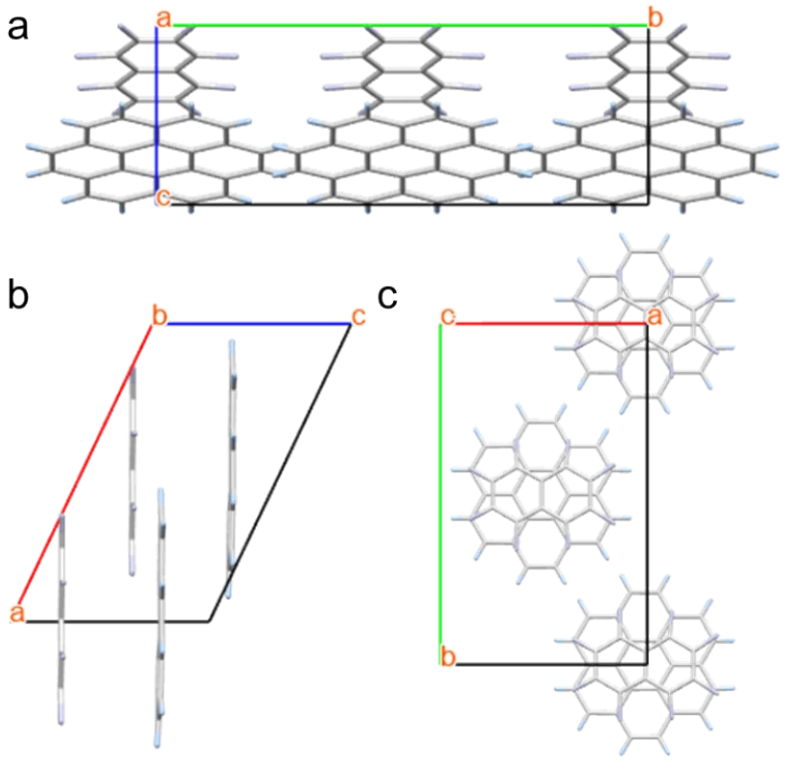

Figure S8. Cell structure of OFN-Cor. (a) From the a-axis, (b) from the b-axis, and (c) from the c-axis.

Table S1. Cell parameters of OFN-Phe, OFN-Py and OFN-Cor.

	OFN-Phe	OFN-Py	OFN-Cor
a/Å	6.776(2)	6.725(1)	11.403(11)
b/Å	18.180(6)	8.864(1)	16.99(2)
c/Å	7.666(3)	9.488(1)	6.872(6)
α/°	90	107.51(1)	90
β/°	102.45(1)	105.23(1)	115.524(10)
γ/°	90	106.82(1)	90
Space Group	P 21/n (14)	P $\bar{1}$ (2)	Cm (8)

Table S2. Crystal data and structure refinement for OFN-Phe.

CCDC Deposition Number	2487236
Empirical formula	$C_{24}H_{10}F_8$
Formula weight	450.32
Temperature/K	100.00(10)
Crystal system	monoclinic
Space group	$P2_1/n$
a/Å	6.7508(3)
b/Å	18.1743(10)
c/Å	7.6426(5)
α/°	90
β/°	102.457(6)
γ/°	90
Volume/Å^3	915.59(9)
Z	2
ρcalcg/cm^3	1.633
μ/mm^{-1}	1.343
F(000)	452.0
Crystal size/mm^3	0.26 × 0.23 × 0.17
Radiation	Cu Kα (λ = 1.54184)
2Θ range for data collection/°	9.734 to 152.318
Index ranges	$-5 \leq h \leq 7$, $-22 \leq k \leq 22$, $-9 \leq l \leq 9$
Reflections collected	3942
Independent reflections	3942 [R_{sigma} = 0.0056]
Data/restraints/parameters	3942/4/185
Goodness-of-fit on F^2	1.030
Final R indexes [I>=2σ (I)]	R_1 = 0.0724, wR_2 = 0.2183
Final R indexes [all data]	R_1 = 0.0777, wR_2 = 0.2270
Largest diff. peak/hole / e Å^{-3}	0.27/-0.31

6. Powder X-ray Diffraction (PXRD)

Powder X-ray diffraction (PXRD) measurements were performed using a Rigaku SmartLab diffractometer (Japan) at the Tianjin Key Laboratory of Molecular Optoelectronic Sciences. The instrument was operated with Cu Kα radiation (λ = 1.5418 Å), at 45 kV and 200 mA, with a total power of 9 kW. Single-component molecular samples were purchased commercially, ground uniformly, and used without further purification. Cocrystal powders were prepared via liquid-assisted grinding and directly subjected to PXRD analysis.

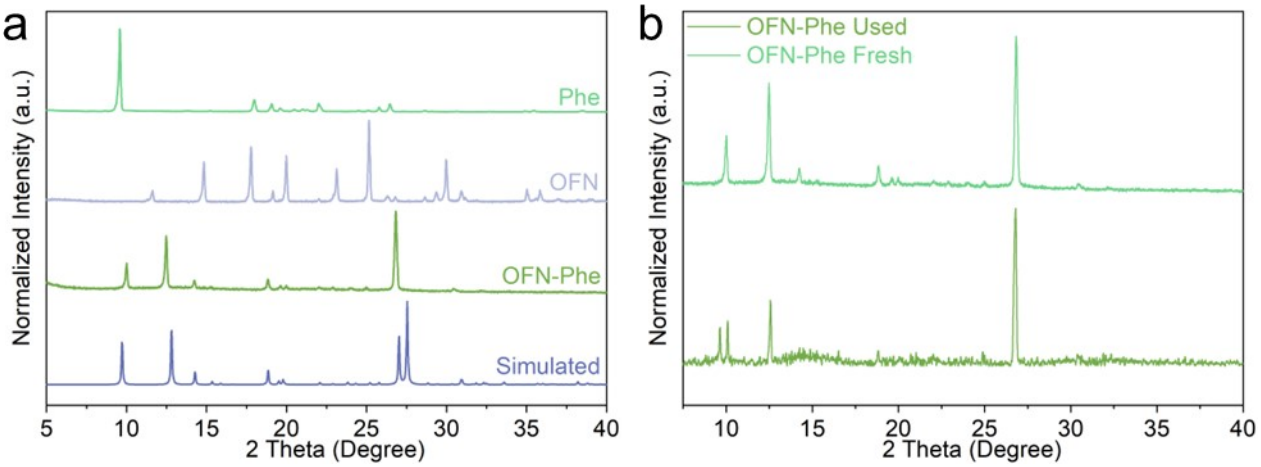

Figure S9. (a) The PXRD results of Phe, OFN, and OFN-Phe, and calculated XRD pattern from the CIF file. (b) PXRD of OFN-Phe before and after using as photocatalyst for pollutant degradation.

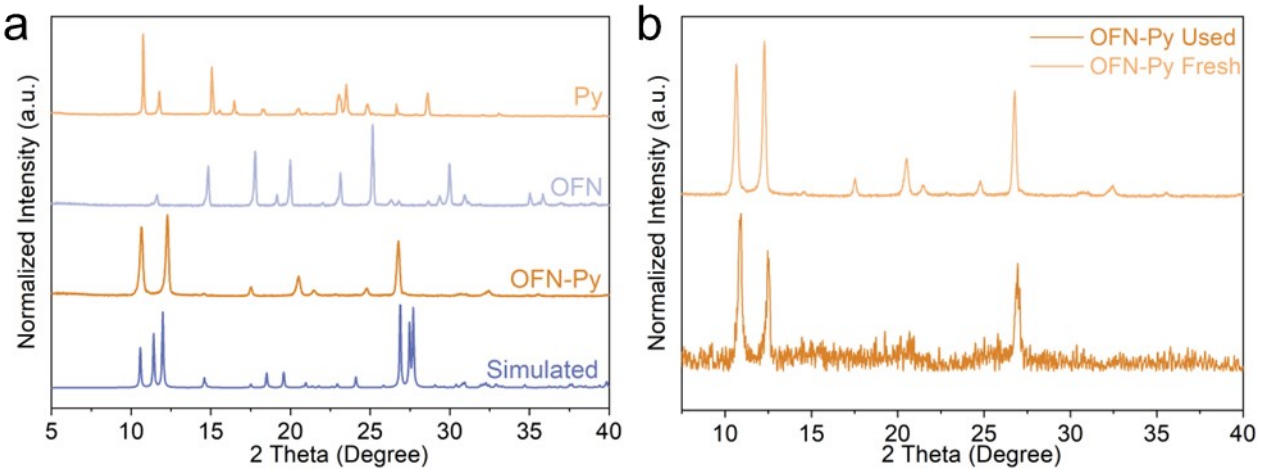

Figure S10. (a) The PXRD results of Py, OFN, and OFN-Py, and calculated XRD pattern from the CIF file. (b) PXRD of OFN-Py before and after using as photocatalyst for pollutant degradation.

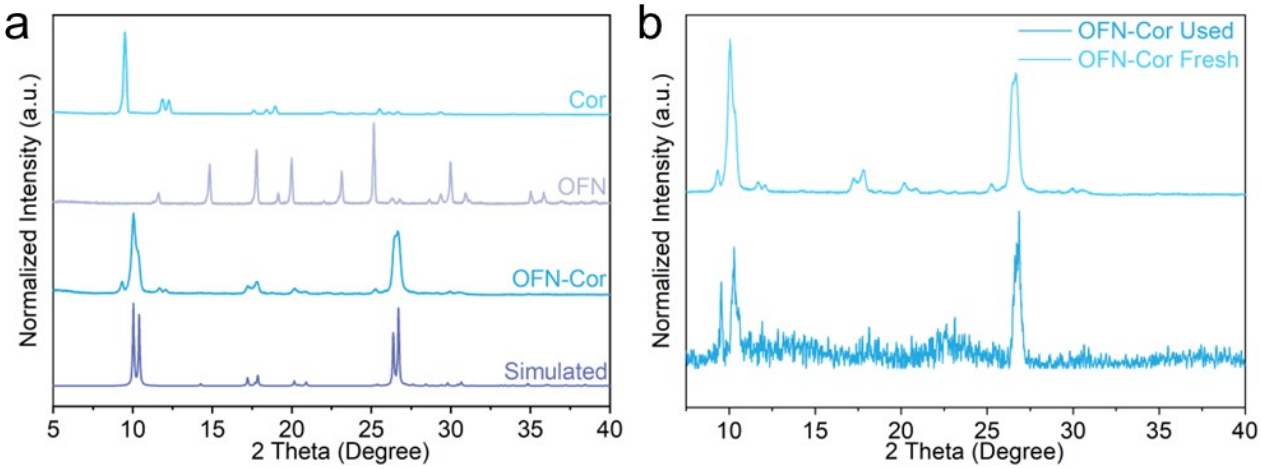

Figure S11. (a) The PXRD results of Cor, OFN, and OFN-Cor, and calculated XRD pattern from the CIF file. (b) PXRD of OFN-Cor before and after using as photocatalyst for pollutant degradation.

7. Solid-state ^{13}C NMR and ^{19}F NMR spectra

Solid-state ^{13}C NMR and ^{19}F NMR spectra were acquired using an instrument model JEOL JNM ECZ600R (Interdisciplinary Platform NMR Center), manufactured in Japan, operating at 600 MHz. The single-component molecules used for measurements were purchased directly from a reagent company, properly ground, and not subjected to any purification process. The cocrystal powder was obtained directly through liquid-assisted grinding for testing.

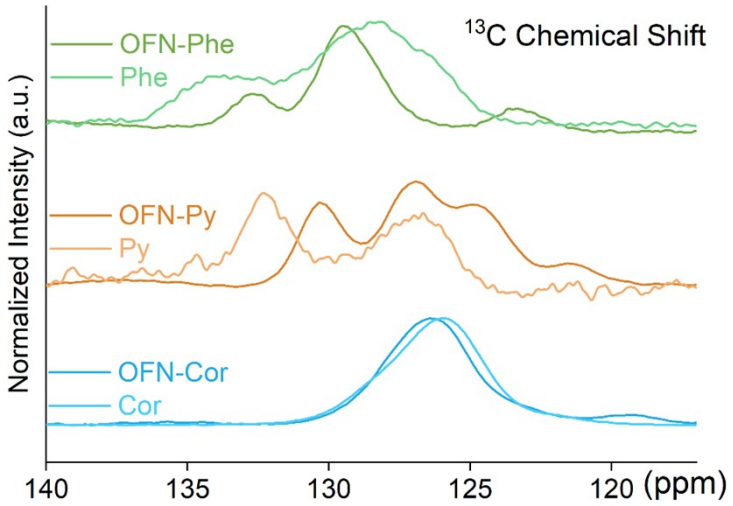

Figure S12. Solid-state ^{13}C-NMR of Phe, Py, Cor, OFN-Phe, OFN-Py and OFN-Cor.

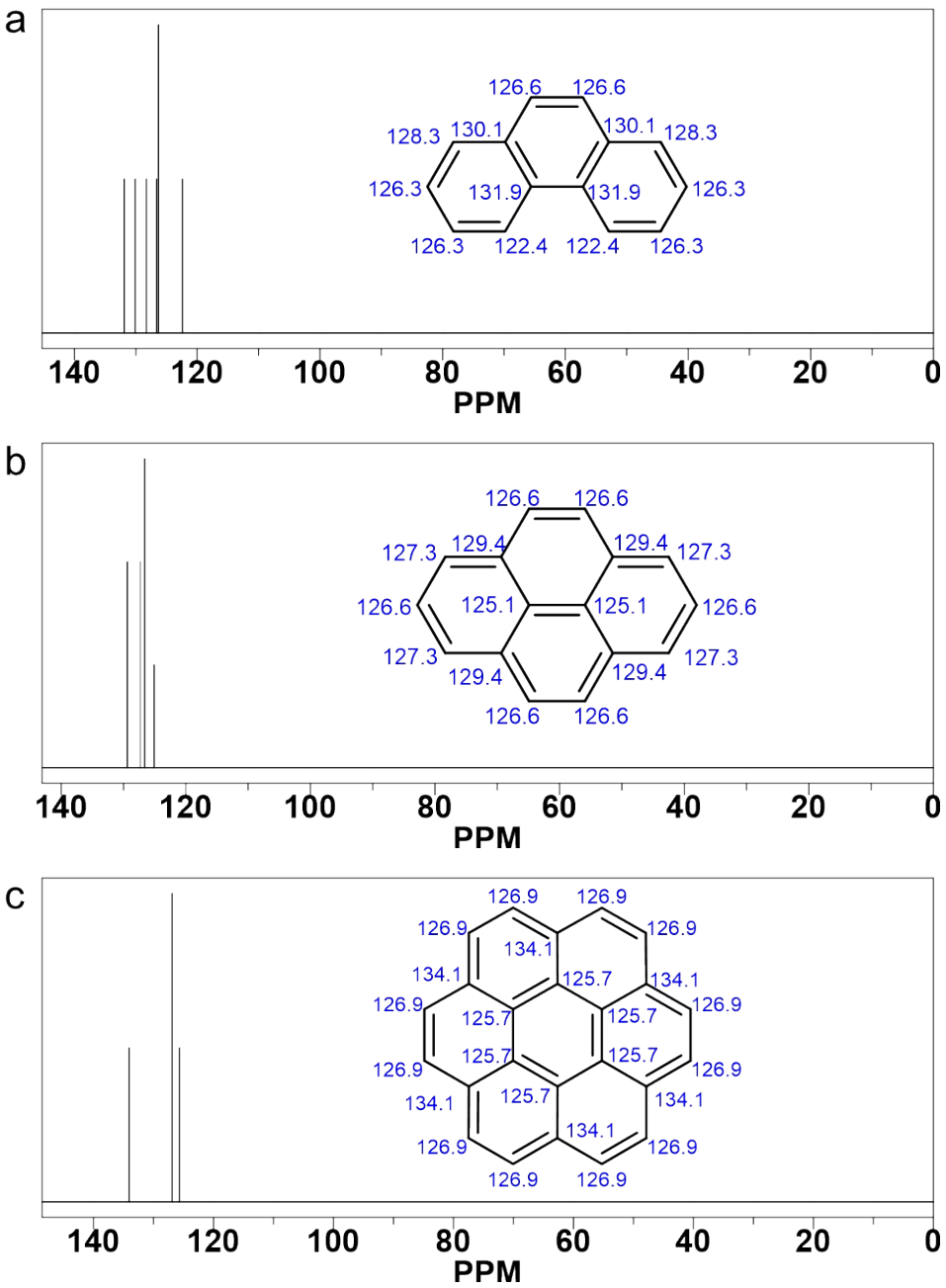

Figure S13. The predicted ^{13}CNMR spectra of Phe, Py and Cor using ChemDraw software (Level: Professional; Version: 23.1.1).

The chemical shift values of the monomer carbon atoms were simulated using ChemDraw software to qualitatively determine the relative electron cloud density of carbon atoms in different chemical environments.

8. Fourier transform infrared (FTIR) Spectroscopy

FTIR spectra were recorded on a Vertex 70 spectrometer (Bruker, Germany) at the Tianjin Key Laboratory of Molecular Optoelectronic Sciences using the attenuated total reflection (ATR) mode[3]. Prior to measurement, the solid powders were dried on a heating stage at 60 °C for 3 h to eliminate residual moisture. Single-component powdered samples were directly purchased from chemical reagent companies, while cocrystal powdered samples were obtained directly through liquid-assisted grinding for testing.

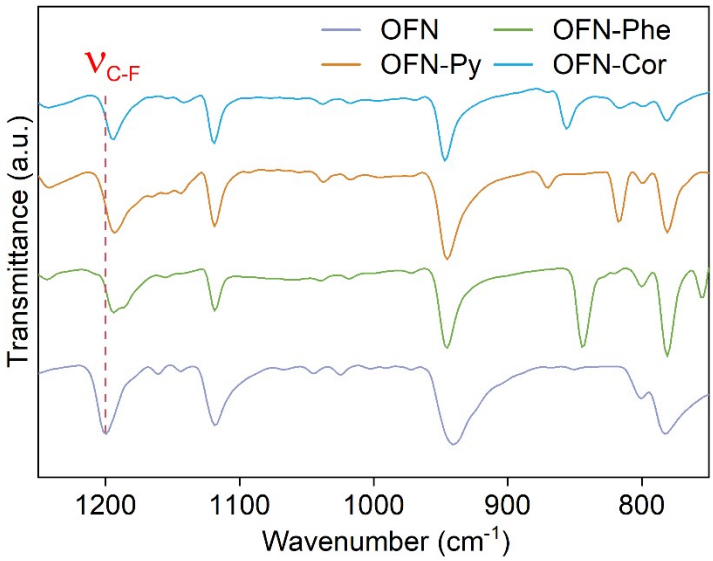

Figure S14. The FTIR spectra of OFN and three cocrystals.

9. UV-Vis absorption spectroscopy

Diffuse reflectance UV-vis spectra were collected on a UV-3600 Plus spectrophotometer (SHIMADZU, Japan) equipped with an integrating sphere (Tianjin Key Laboratory of Molecular Optoelectronic Sciences). Powder samples-either commercially sourced single-component molecules (ground and used without further purification) or cocrystals prepared by liquid-assisted grinding-were evenly dispersed on a $BaSO_4$ substrate. Baseline correction was performed with blank $BaSO_4$ to eliminate substrate contributions. The reflectance data were converted to absorption spectra via the Kubelka-Munk function for subsequent analysis.

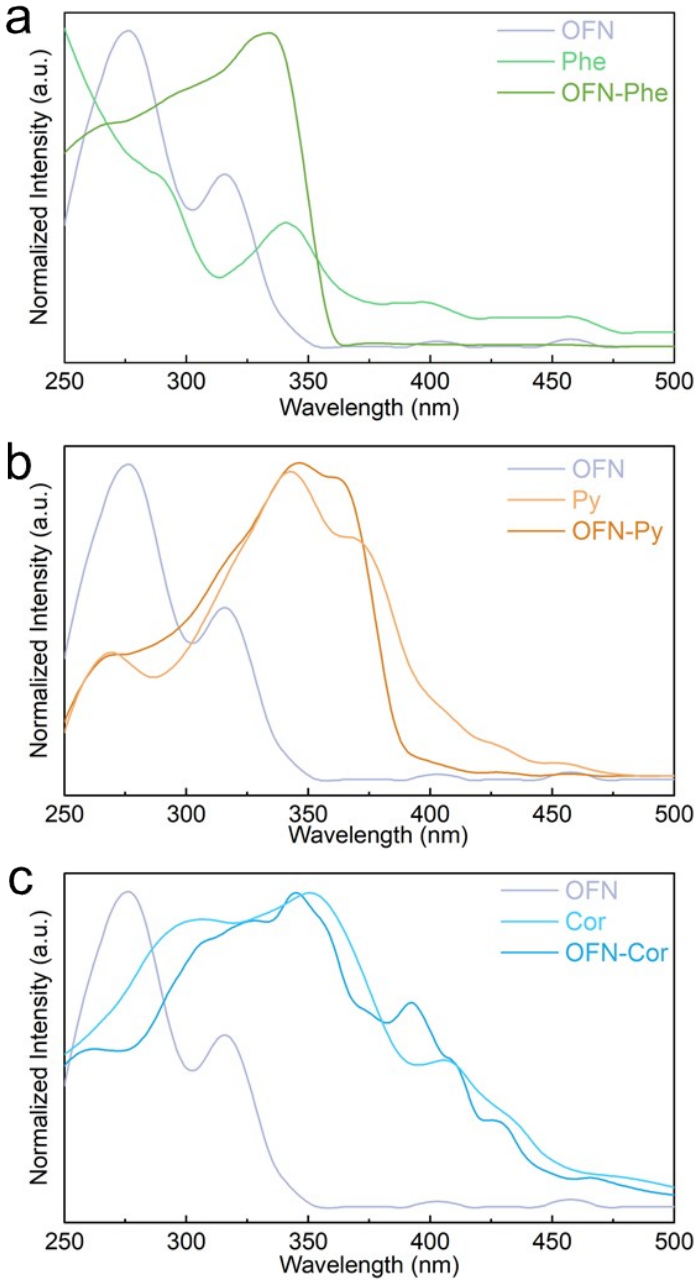

Figure S15. UV-vis spectra of monomeric molecules and cocrystals.

10. Ultraviolet Photoelectron Spectroscopy (UPS)

The ultraviolet photoelectron spectroscopy (UPS) was performed to measure the band structure of photocatalysts. UPS measurements were carried out on a Thermo Scientific Escalab 250Xi spectrometer (School of Materials Science and Engineering, Nankai University). He I was used as the excitation source with an energy of 21.22 eV. Gold specimens (Fermi edge at 0.0 eV) were used to calibrate the instrument. The highest occupied orbit (HOMO) is calculated from the following equation[4]

$$-\text{HOMO} = h\nu - (E_{cutoff} - E_{onset})$$

where $h\nu$ is the photoenergy of He I source (21.22 eV), E_{onset} is binding energy onset, E_{cutoff} is binding energy cutoff.

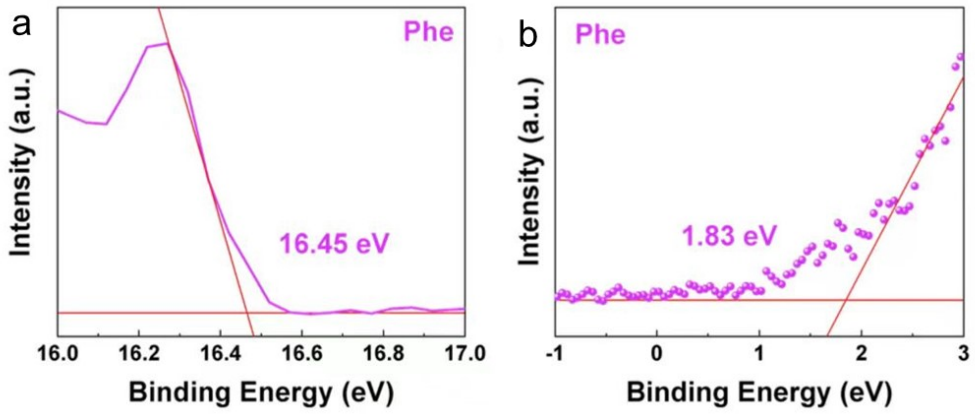

Figure S16. UPS energy spectra of Phe crystal.

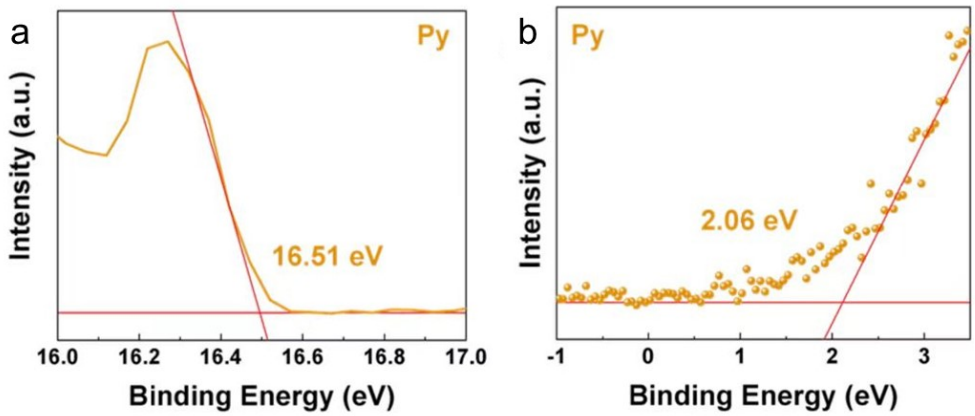

Figure S17. UPS energy spectra of Py crystal.

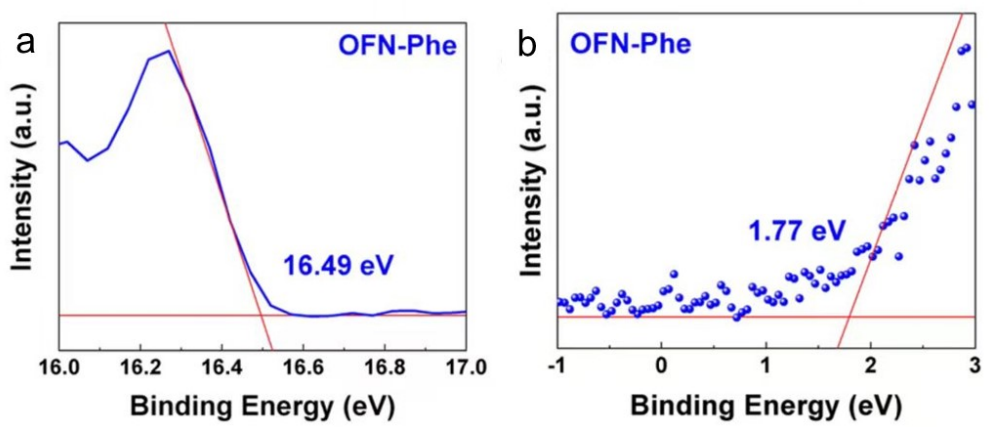

Figure S18. UPS energy spectra of OFN-Phe cocrystal.

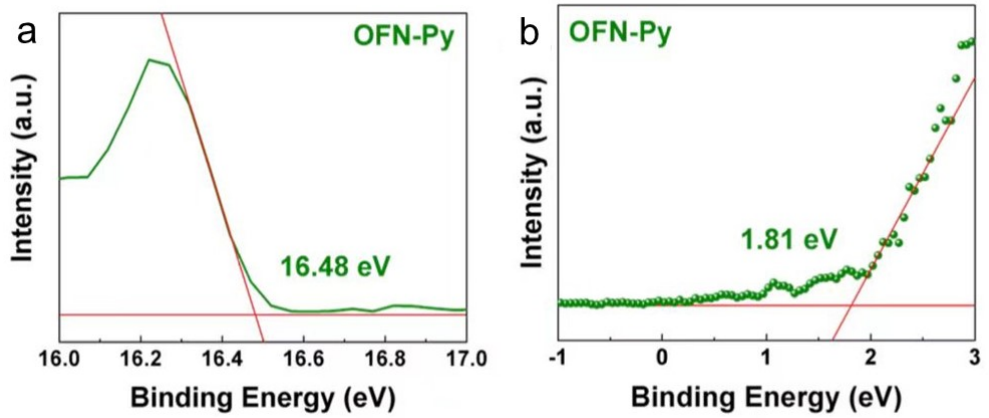

Figure S19. UPS energy spectra of OFN-Py cocrystal.

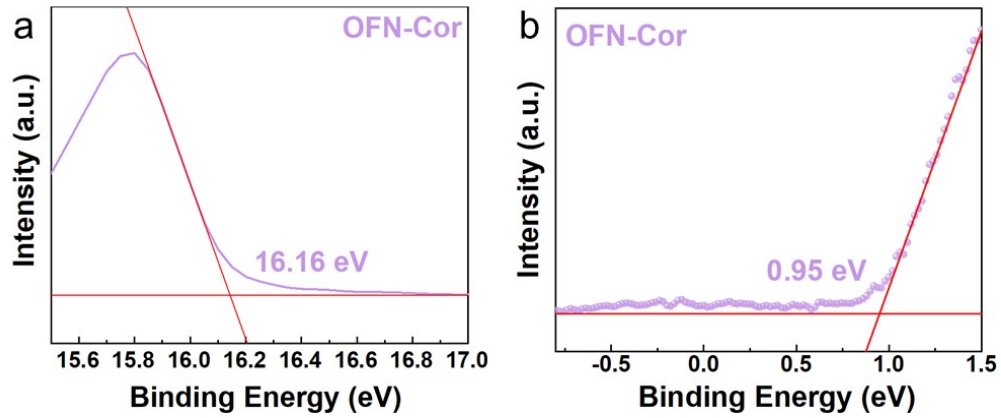

Figure S20. UPS energy spectra of OFN-Cor cocrystal.

Table S3. Summary of HOMO, LUMO and bandgap, calculated from UPS spectra and UV-vis spectra.

	Cutoff tail [eV]	Fermi tail [eV]	*E*g [eV]	HOMO [eV]	LUMO [eV]	CB [eV]	VB [eV]
OFN[5]	16.35	1.45	3.67	-6.32	-2.65	1.82	-1.85
Phe	16.45	1.83	3.29	-6.6	-3.31	2.1	-1.19
OFN-Phe	16.49	1.77	3.48	-6.5	-3.02	2	-1.48
Py	16.51	2.06	3.04	-6.77	-3.73	2.27	-0.77
OFN-Py	16.48	1.81	3.21	-6.55	-3.34	2.05	-1.16
Cor[6]	16.26	0.56	2.79	-5.52	-2.73	1.02	-1.77
OFN-Cor	16.16	0.95	2.93	-6.01	-3.08	1.51	-1.42

11. Photoluminescence spectroscopy and fluorescence decay lifetime

The PL spectrum was acquired using the F7000 FL (Japan) spectrophotometer (Tianjin Key Laboratory of Molecular Optoelectronic Sciences). The Edinburgh FLS1000 fluorescence spectrometer (Institute of Molecular Aggregation Science, Tianjin University) was used to measure the lifetime (τ). And nF920 nanosecond lamp and an EPL-375 3B laser were used for fluorescence lifetime measurements. The decay curve was well described by a single-exponential function, $y = A \cdot exp(-x/\tau) + C$[7], where A denotes the prefactor and C represents a constant. The carrier lifetime (τ) was subsequently determined through automated data fitting. Cocrystal powdered samples were obtained directly through liquid-assisted grinding for testing.

12. Femtosecond transient absorption spectroscopy (Fs-TA)

Femtosecond transient absorption (Fs-TA) measurements were performed at the Technical Institute of Physics and Chemistry, Chinese Academy of Sciences, using a regenerative-amplified Ti:sapphire laser system (Legend Elite-1K-HE, Coherent) coupled with a Helios pump-probe spectrometer (Ultrafast Systems). The laser system delivered pulses centered at 800 nm with a pulse duration of 25 fs, pulse energy of 4 mJ, and a repetition rate of 1 kHz. The fundamental 800 nm output was split into two beams: the major portion was directed into an optical parametric amplifier to generate the pump pulses, while the remaining portion was used to generate the white-light probe continuum in the TA spectrometer[7].

Sample preparation: An amount of the sample was dispersed in an ethanol-water co-solvent system and sonicated to form a uniform and stable suspension, which was used for subsequent experimental measurements.

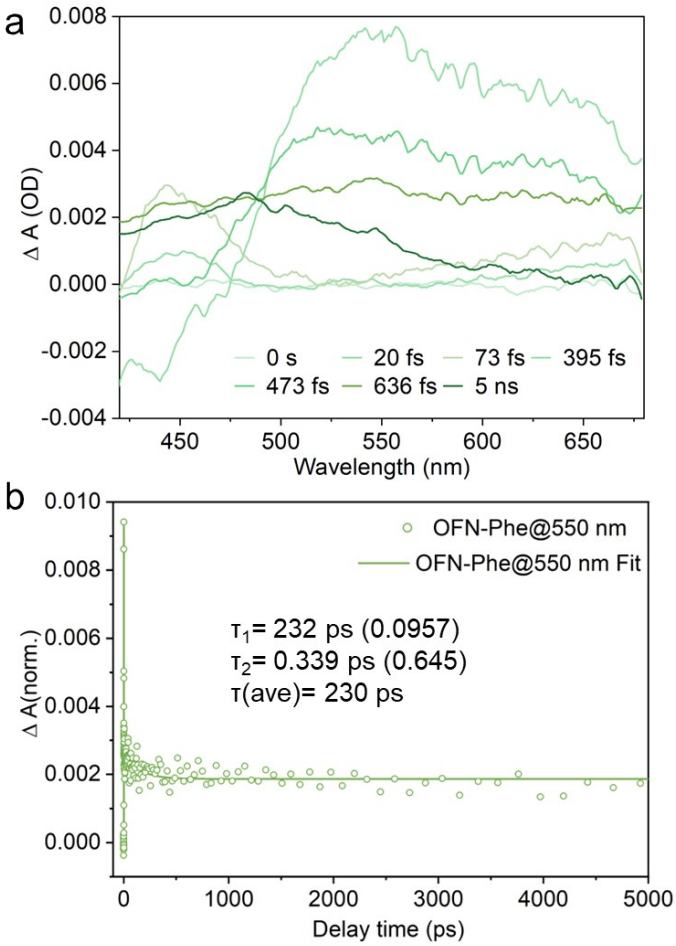

Figure S21. (a) Fs-TA spectrum versus pump-probe delay time for OFN-Phe. (b) Decay kinetic curve of OFN-Phe.

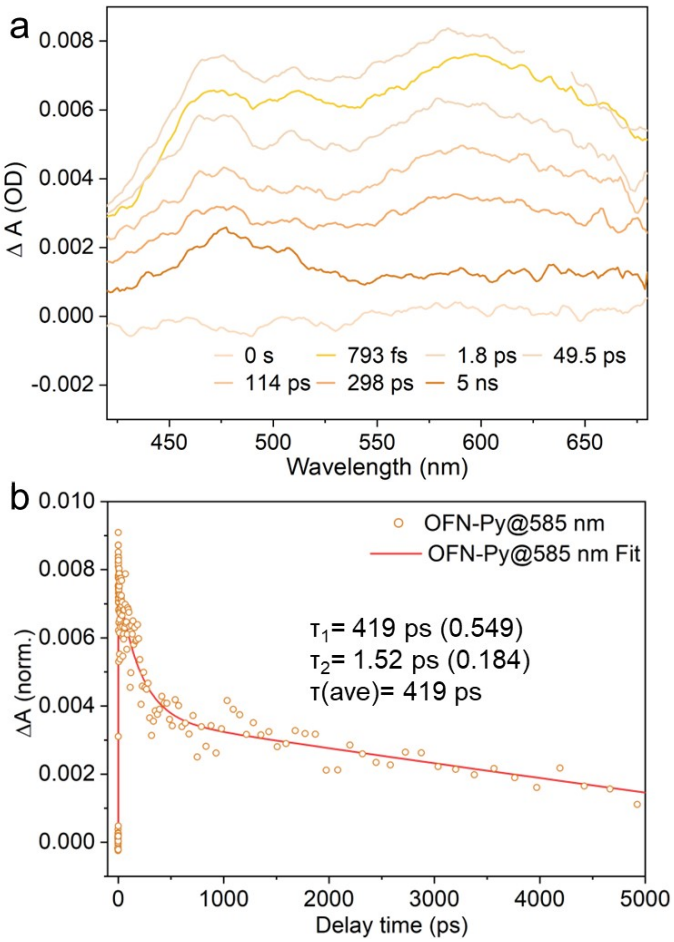

Figure S22. (a) Fs-TA spectrum versus pump-probe delay time for OFN-Py. (b) Decay kinetic curve of OFN-Py.

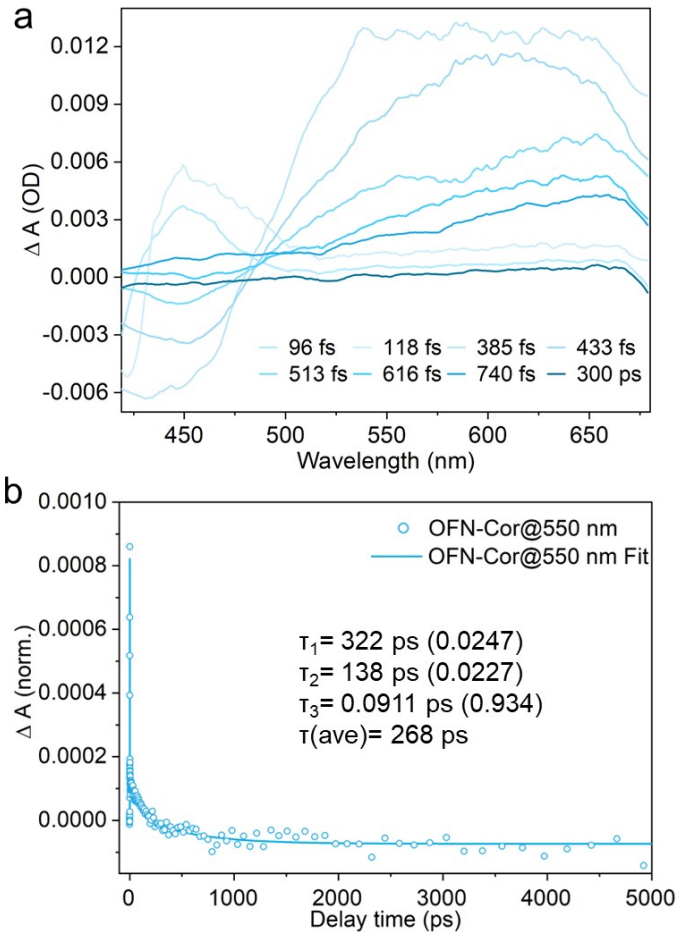

Figure S23. (a) Fs-TA spectrum versus pump-probe delay time for OFN-Cor. (b) Decay kinetic curve of OFN-Cor.

13. Transient Electron Paramagnetic Resonance (Tr-EPR) Spectroscopy

Tr-EPR experiments were conducted on a Bruker EMX spectrometer, equipped with an ER-4118CV liquid nitrogen cryostat kept at 110K and an ER-4118X-MS5 split-ring resonator tuned and matched to critical coupling for each sample (Q ~ 2000). 355 mm laser pulses with ~10 ns duration and 2 mJ energy were repeated at 10 Hz rate. Powder samples were sealed in argon atmosphere to avoid photobleaching. The transient signal, which is a time trace of 16 μs length (8 ns × 2000 points), was recorded after each excitation. 201 magnetic field points evenly distributed between 2500 - 4300 gauss were sampled, each with 250 transient traces collected and averaged to improve signal-to-noise ratio. The microwave excitation power was 2 mW.

Spectral simulations were generated using the EasySpin software package[8], version 6.0.5 with MATLAB R2024b. A linear background was removed along the magnetic field axis for each time point, the remaining signal in the time window of 0.8 - 2 μs was integrated to generate the spectra in **Fig. 3j** of the Main Text. A cubic polynomial function was used as baseline for the simulations, and Nelder-Mead downhill simplex method was used for fitting the simulations to the experimental spectra. Fitted simulation parameters: OFN-Phe: microwave frequency 9.5180 GHz, triplet sublevel populations [0.5, 0.5, 0] in the [T_x, T_y, T_z] basis, g = 2.013, D = 1452 MHz, E = 332 MHz; OFN-Py: microwave frequency 9.50981 GHz, sublevel populations [0, 1, 0] in the [T_{-1}, T_0, T_{+1}] basis, g = 2.011, D = -2077 MHz, E = 341 MHz; OFN-Cor: microwave frequency 9.5223 GHz, sublevel populations [0.5, 0.5, 0] in the [T_x, T_y, T_z] basis, g = 2.012, D = 1990 MHz, E = 251 MHz.

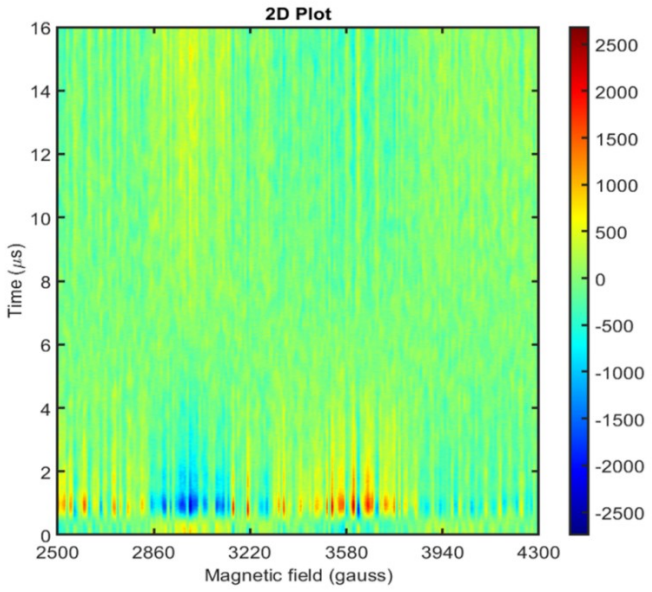

Figure S24. Tr-EPR spectrum recorded for OFN-Phe.

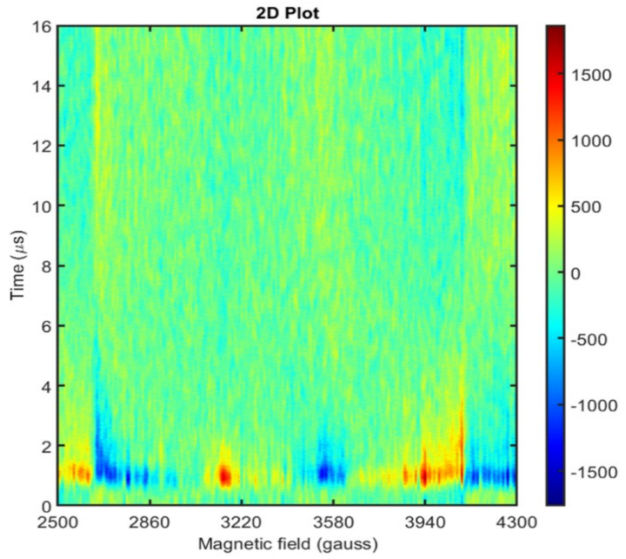

Figure S25. Tr-EPR spectrum recorded for OFN-Py.

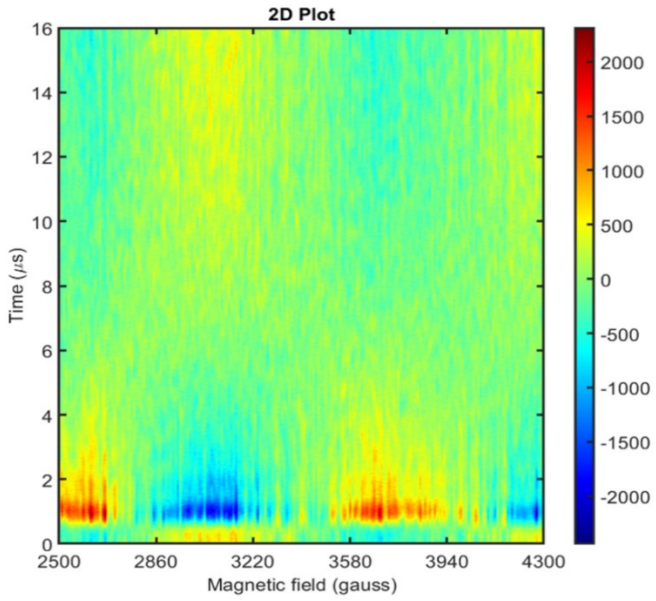

Figure S26. Tr-EPR spectrum recorded for OFN-Cor.

14. Kelvin Probe Force Microscopy (KPFM)

Kelvin Probe Force Microscopy (KPFM) was performed on a Bruker Dimension Icon microscope (Tianjin Key Laboratory of Molecular Optoelectronic Sciences) under ambient atmosphere in the amplitude-modulated (AM-KPFM) mode. The test procedure as follows: THF solutions of OFN-Phe, OFN-Py and OFN-Cor (0.25 mg mL^{-1}) were dropped on bare Si substrate to obtain micro-nano crystals. During the measurement of surface potential, the lift mode was used with a lift height of 100 nm. The obtained data were processed using NanoScope Analysis software to obtain surface potential images and the corresponding contact potential.

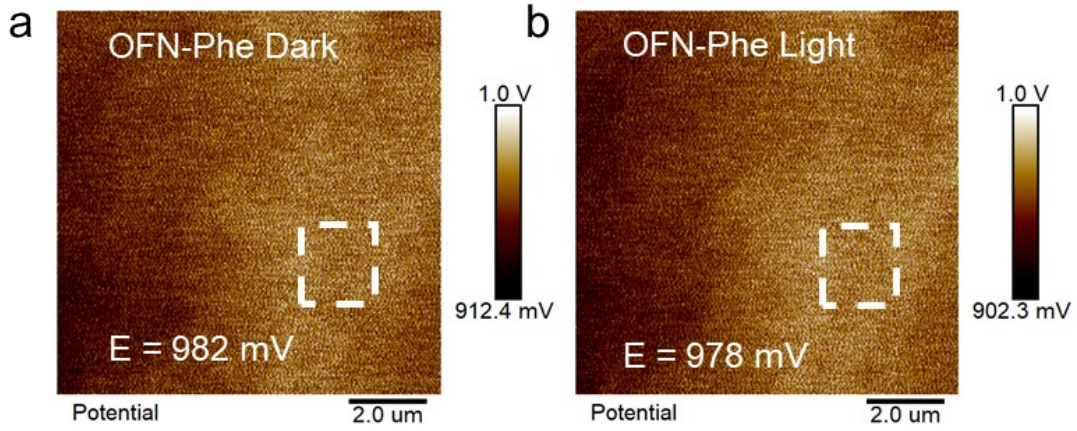

Figure S27. Surface potential of OFN-Phe under (a) dark-field and (b) bright-field conditions detected by KPFM.

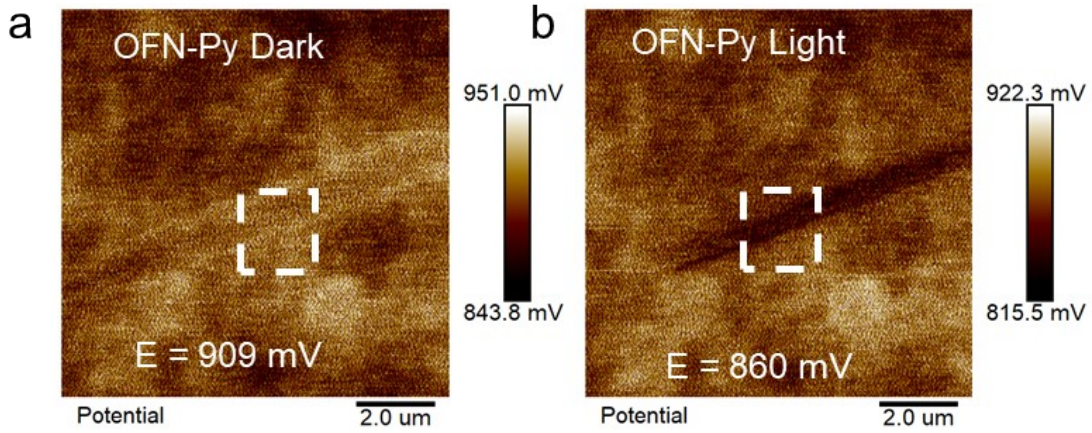

Figure S28. Surface potential of OFN-Py under (a) dark-field and (b) bright-field conditions detected by KPFM.

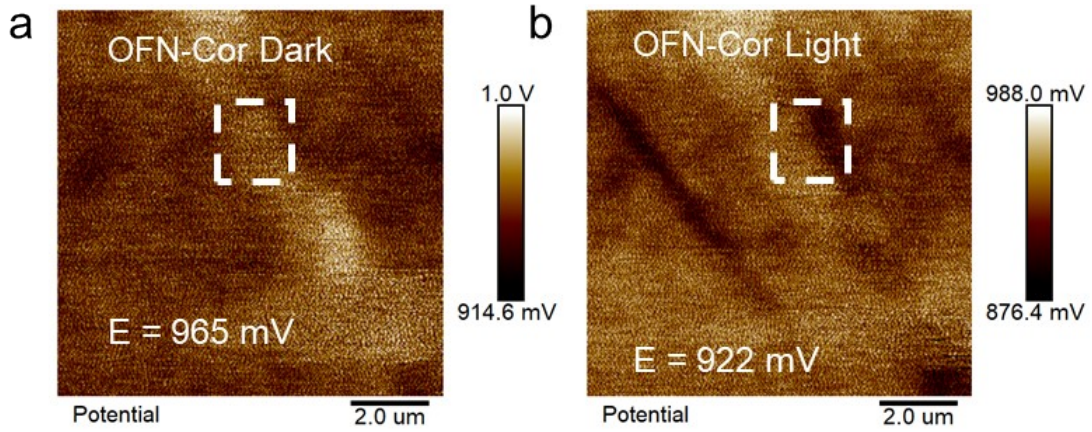

Figure S29. Surface potential of OFN-Cor under (a) dark-field and (b) bright-field conditions detected by KPFM.

15. Photocurrent test

The photoelectrochemical properties of the cocrystal catalysts were measured using a CHI760E electrochemical workstation (Shanghai Chenhua, China) at the Tianjin Key Laboratory of Molecular Optoelectronic Sciences. A three-electrode system was employed for this study, consisting of an ITO glass (2.5 × 2.5 cm^2) coated with the photocatalyst as the working electrode, a platinum plate (1.0 × 1.0 cm^2) as the counter electrode, and a standard Ag/AgCl electrode ($E_{Ag/AgCl}$ = 0.210 V vs NHE) as the reference electrode. A 0.5 M Na_2SO_4 aqueous solution was used as the electrolyte, and a 300 W Xe lamp (PLS-SXE300D, Beijing Perfectlight) served as the light source. The working electrode was prepared by ultrasonically dispersing the photocatalyst sample in 1 mL of a water/ethanol mixture (v/v = 1:1) to form a homogeneous suspension with a concentration of 3 mg mL^{-1}. Then, 10 μL of Nafion solution was added as a binder. And the resulting suspension was drop-cast onto an ITO glass substrate and subsequently dried at room temperature for 12 h.

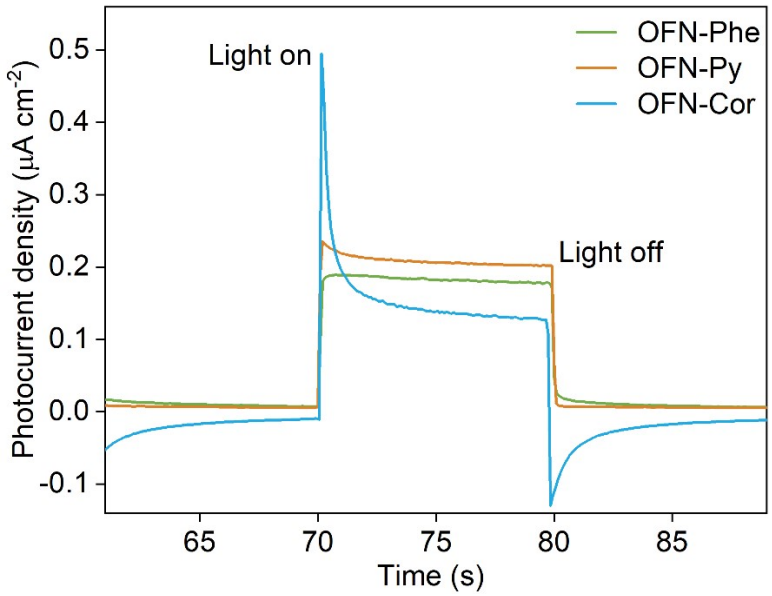

Figure S30. Transient photocurrent-time curves.

16. Photocatalytic Measurements

(1) Photocatalytic degradation experiment

The photocatalytic performance of the samples was evaluated by degrading common benzene series compounds, such as phenol and aniline. Prior to the photocatalytic experiment, a 60-minute dark treatment was conducted to achieve adsorption-desorption equilibrium. During the photocatalytic experiment, a double-layer jacketed beaker with circulating cooling water was employed to maintain a constant reaction temperature under irradiation from a 300 W Xe lamp (Perfect Light, PLS-SXE300D/300DUV). Oxygen was continuously supplied at 50 mL/min to enhance the efficiency of pollutant degradation.

The specific procedure was as follows: 25 mg of photocatalytic material was dispersed in 50 mL of pollutant solution (20 ppm) and stirred with ultrasonic treatment to form a uniformly dispersed suspension. After 60 minutes of dark treatment to reach adsorption-desorption equilibrium, the photocatalytic reaction was initiated. A 2 mL sample was taken every 30 minutes, and the sample solution was filtered through a 0.22 μm microporous membrane to remove solid catalysts, yielding a clear liquid.

The pollutant concentration was determined using high-performance liquid chromatography (HPLC, Waters E2695 Separation Module coupled with a 2998 PDA detector) on a C18 reversed-phase column[7]. The degradation efficiency was expressed as C_t/C_0, where C_t represented the pollutant concentration at a given sampling time, and C_0 represented the concentration after adsorption equilibrium in the dark.

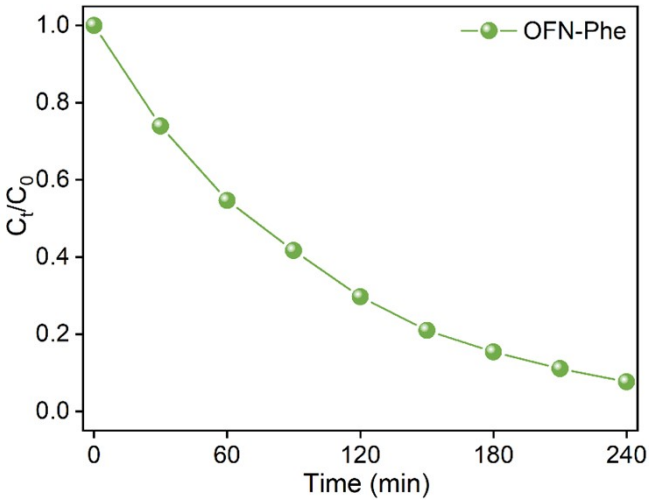

Figure S31. The photocatalytic degradation curves of phenol by OFN-Phe.

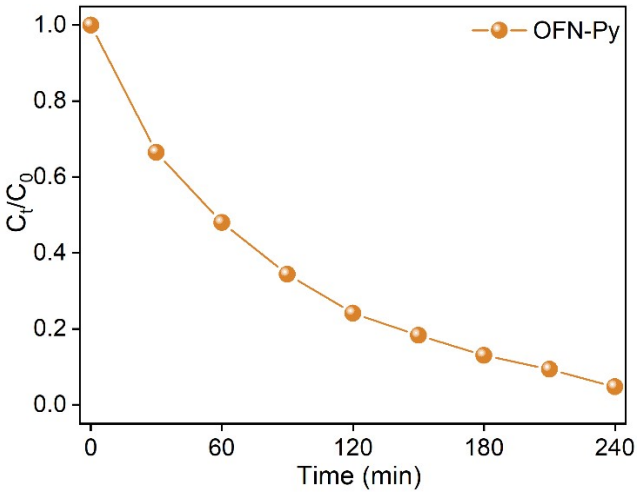

Figure S32. The photocatalytic degradation curves of phenol by OFN-Py.

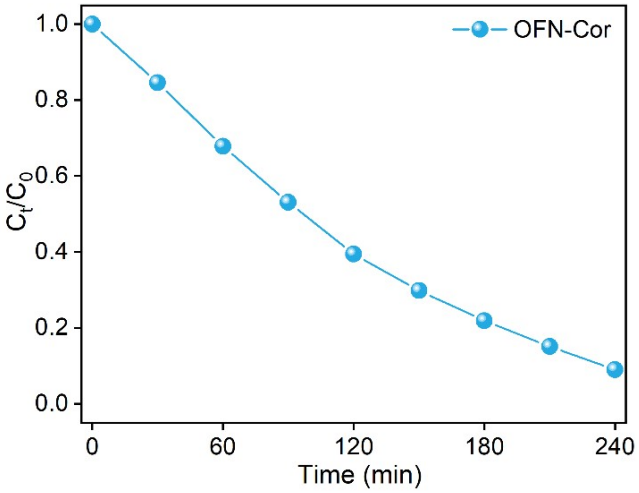

Figure S33. The photocatalytic degradation curves of phenol by OFN-Cor.

Table S4. Comparative performance of semiconductor photocatalytic degradation of phenol.

Photocatalysts	Concentration [ppm]	Time [h]	Degradation Rate [%]	References
SA-PDINH	5	8	46	[9]
SA-PDI	5	3	48	[10]
Nano PDI	5	8	66	[11]
PDI/O-CN-40%	5	4	52	[12]
50%-Bi_2WO_6/PDI	5	3	68	[10]
hp-PDI-NA	10	6	100	[13]
NDI-Cor	20	4	100	[6]
PDI-SE	10	4	79.3	[14]
TiO_2	50	4	10	[15]
RGO/TiO_2	50	4	25	[15]
0.7%Fe/TiO_2	50	5	35	[16]
OFN-Phe	20	2	70	This work
OFN-Py	20	2	76	This work
OFN-Cor	20	2	61	This work

(2) H_2O_2 photosynthesis

5 mg catalyst and 50 mL water were evenly dispersed in a quartz bottle with avolume of 100 mL and passed into dry O_2, stirred for 30 min under dark conditions toreach adsorption-desorption equilibrium. Then, the photocatalytic reaction was initiated. After sampling every 60 minutes, the solution was filtered through a 0.22 μm filter to detect the content of H_2O_2 in the solution. The H_2O_2 concentration was determined by a potassium titanium oxalate method.

(3) Radical Quenching Experiments

The types of radicals generated during photocatalysis were initially probed by radical quenching experiments. Ascorbic acid (AA), isopropyl alcohol (IPA), and methanol (MeOH) were used as scavengers for·O_2^-, ·OH and h^+ respectively[17]. While the concentrations of IPA and MeOH were set at 10 mM, the concentration of AA was reduced to 2.5 mM to avoid excessive quenching(Figure S17a).

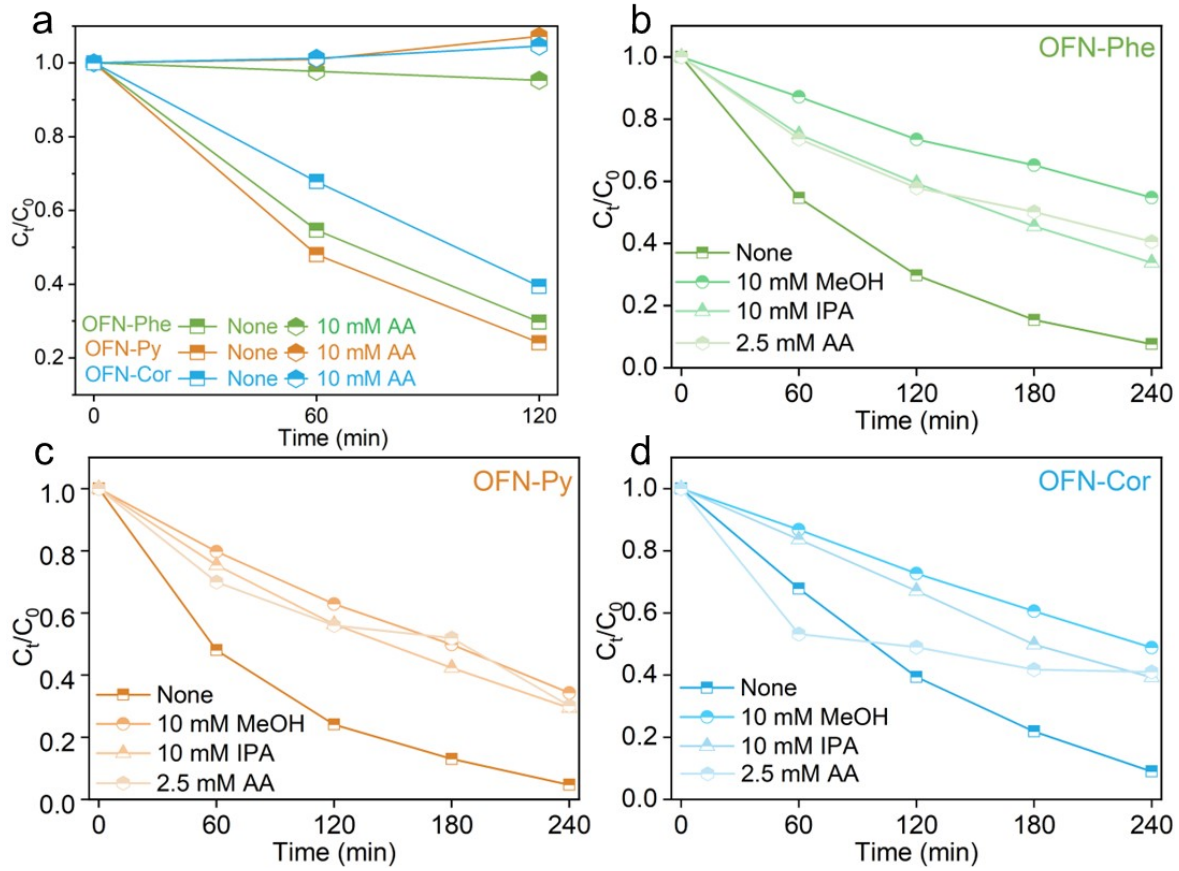

Figure S34. Active radical quenching experiments for phenol degradation of OFN cocrystals. (a) 10 mM AA (b) OFN-Phe. (c) OFN-Py (d) OFN-Cor.

17. Electron Paramagnetic Resonance (EPR) Spectroscopy

Electron paramagnetic resonance (EPR) measurements were performed on a Bruker EMXplus spectrometer at a microwave frequency of 9.42 GHz, with a modulation amplitude of 0.1 mT and a microwave power of 5 mW.

Cocrystal powder samples of equal mass were directly obtained through liquid-assisted grinding for testing. The EPR spectra of OFN-Phe and OFN-Py cocrystal powders exhibit no detectable signals, whereas the OFN-Cor cocrystal powder displayed a very weak EPR response at $g = 2.0049$, which can be ascribed to a tiny amount of semiquinone radicals formed from oxidation of Cor donor molecules[18].

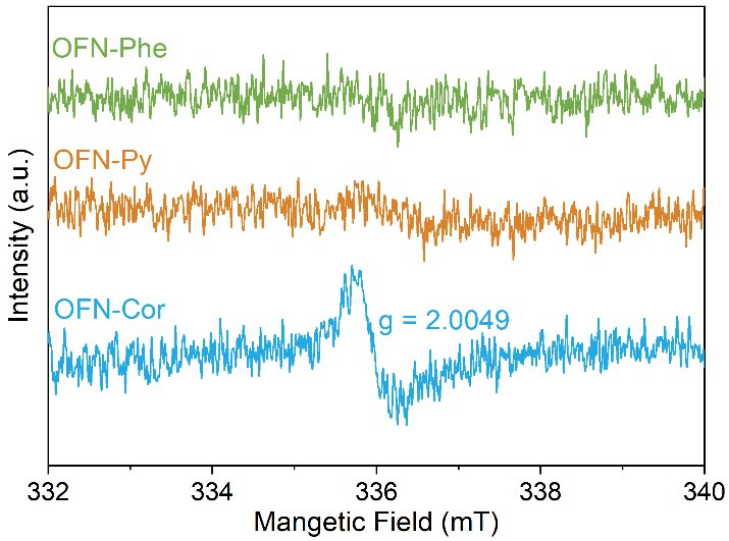

Figure S35. The EPR spectra of OFN-Phe, OFN-Py and OFN-Cor in darkness.

Spin-trapping EPR measurements were conducted to detect the reactive species formed during the catalytic reaction. Sample Preparation: 5,5-dimethyl-1-pyrroline N-oxide (DMPO) or 2,2,6,6-Tetramethylpiperidine-1-oxyl (TEMPO) solutions (100 mM) were prepared in deionized water or acetonitrile to obtain DMPO-H_2O, DMPO-acetonitrile, and TEMPO-acetonitrile solutions. For hydroxyl radical (•OH) detection, 5 mg of sample was mixed with 50 μL of water and 50 μL of DMPO-H_2O solution; for superoxide radical ($•O_2^-$) detection, with 50 μL of acetonitrile and 50 μL of DMPO-acetonitrile solution; and for hole (h^+) detection, with 50 μL of acetonitrile and 50 μL of TEMPO-acetonitrile solution. All mixtures were sonicated for 5 min, covered with aluminum foil, and kept in the dark. During the measurements, the samples were exposed to a 300 W xenon lamp (PLS-SXE300D, Beijing Perfectlight).

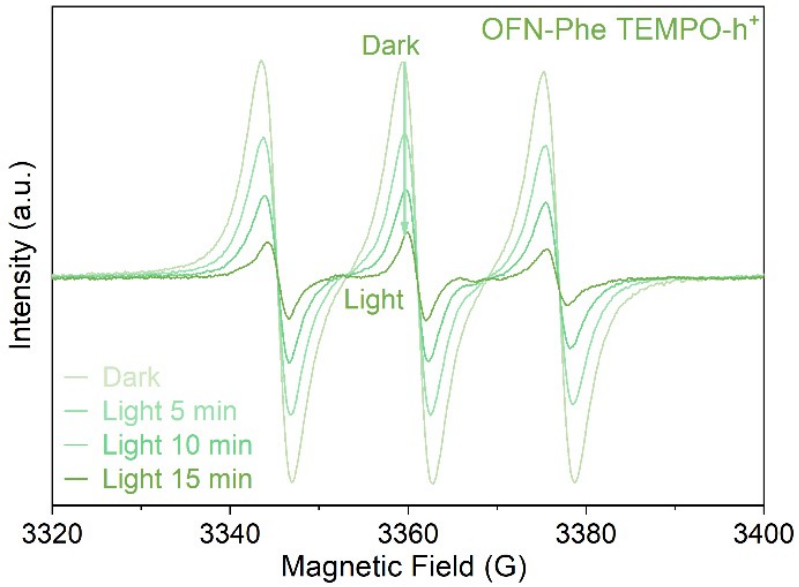

Figure S36. Variation in hole signal intensity of OFN-Phe during photocatalysis under different irradiation times.

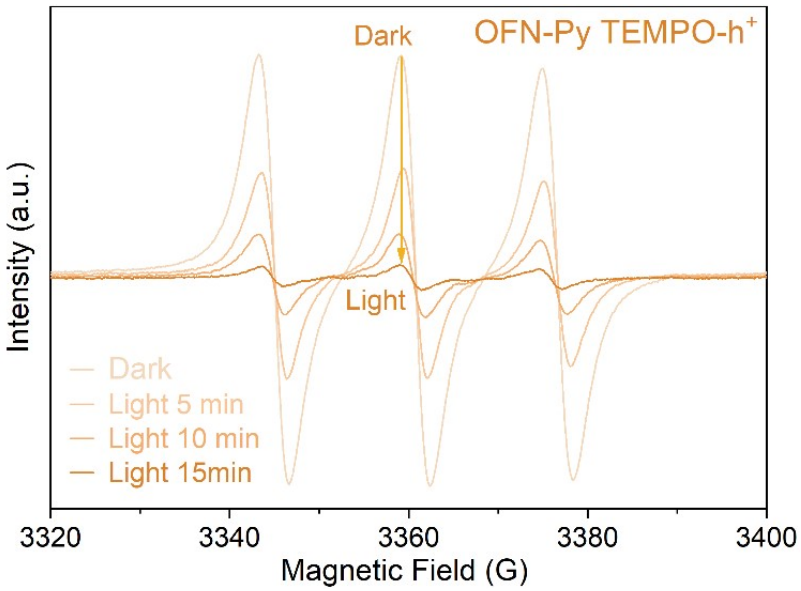

Figure S37. Variation in hole signal intensity of OFN-Py during photocatalysis under different irradiation times.

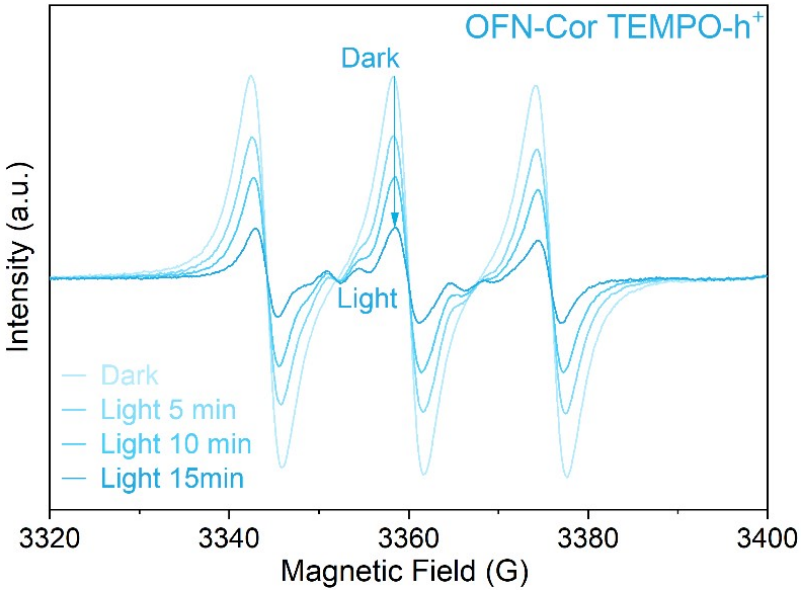

Figure S38. Variation in hole signal intensity of OFN-Cor during photocatalysis under different irradiation times.

18. LC-MS spectra of phenol degradation intermediates

A comprehensive analysis of the final products from the photocatalytic degradation of phenol by OFN-Py (reaction duration: 240 minutes) was carried out using a high-resolution ion mobility quadrupole time-of-flight mass spectrometer (SELECT SERIES Cyclic IMS) at the School of Chemical Engineering and Technology, Tianjin University. High-purity water was used as a blank control. For mass spectrometric detection, both positive ion mode (ESI^+) and negative ion mode (ESI^-) were employed, with a scan range of mass-to-charge ratio (m/z) 50-560[19]. Each analysis lasted 20 minutes. For the liquid chromatography component, a reversed-phase C18 column was used, and gradient elution was applied to achieve effective separation of target compounds in the complex matrix. The column temperature was precisely controlled at 35 ± 0.1°C. Methanol and ultrapure water were used as the mobile phases to ensure optimal retention and resolution of the target products. During LC-MS analysis, the formation of sodium adducts ($[M+Na]^+$) was observed due to the intentional addition of sodium acetate (NaOAc), and the corresponding peaks were considered in the structural assignment[20-22].

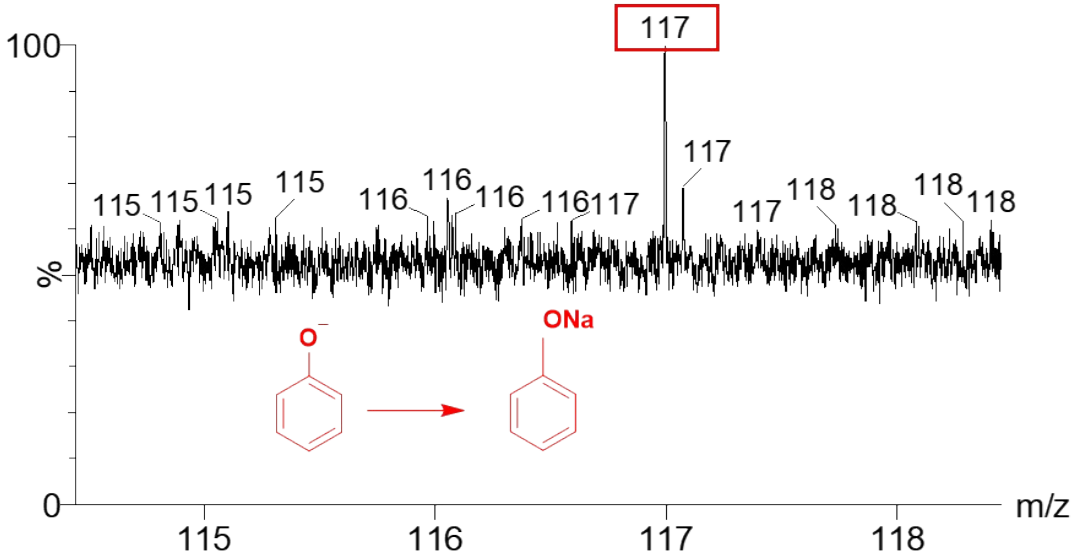

Figure S39. Mass spectrometric analysis of degradation intermediates with the identification of the phenol anion.

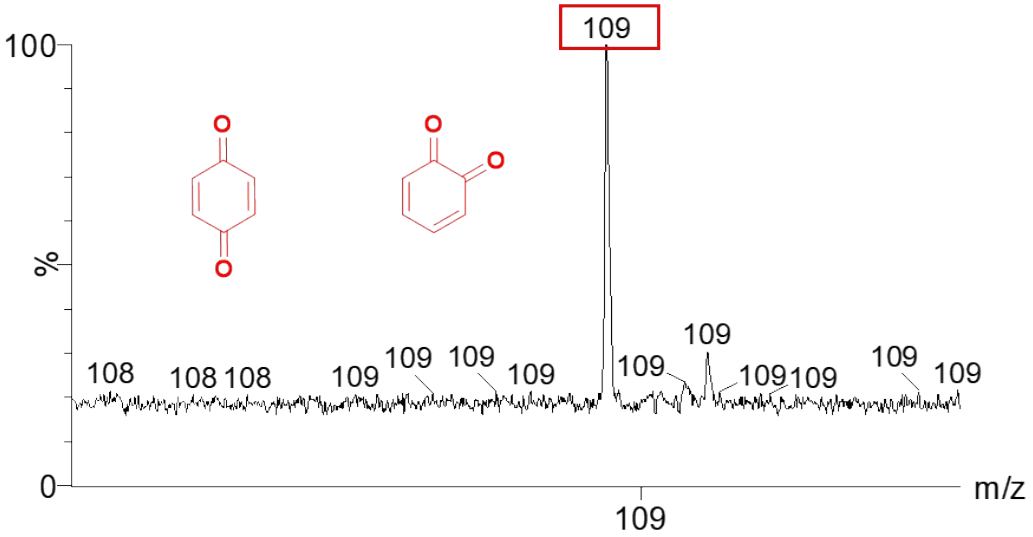

Figure S40. Mass spectrometric analysis of degradation intermediates with the identification of the benzoquinone.

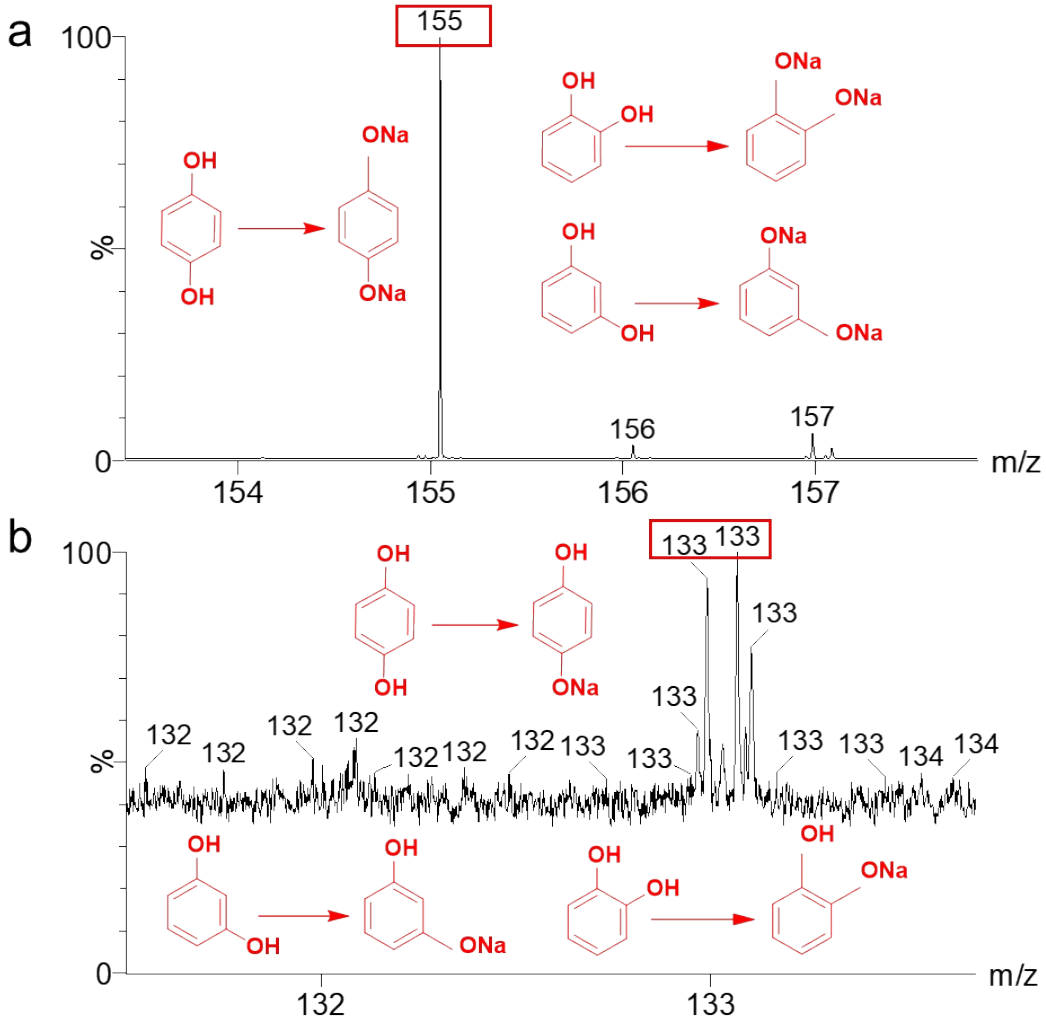

Figure S41. Mass spectrometric analysis of degradation intermediates with the identification of the phenol anion.

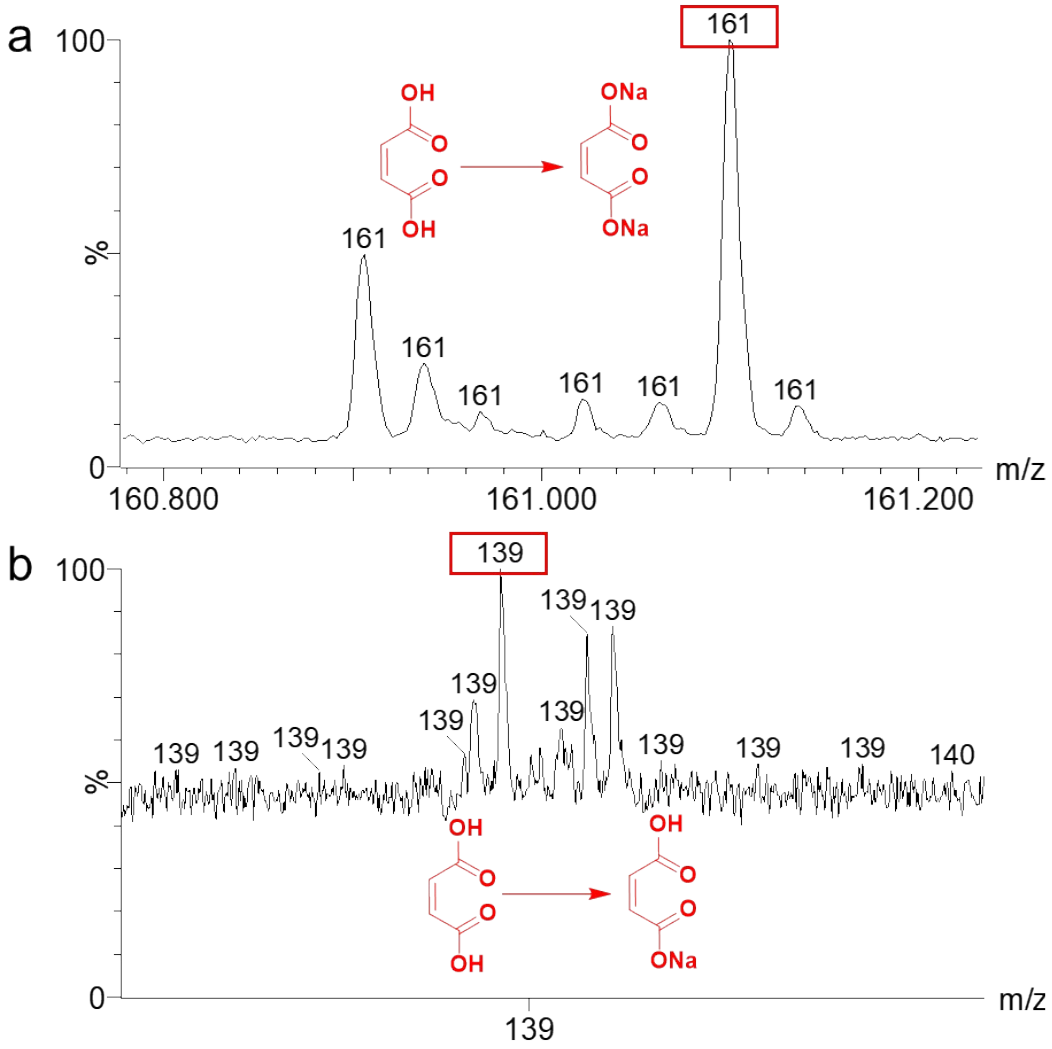

Figure S42. Mass spectrometric analysis of degradation intermediates with the identification of the maleic acid.

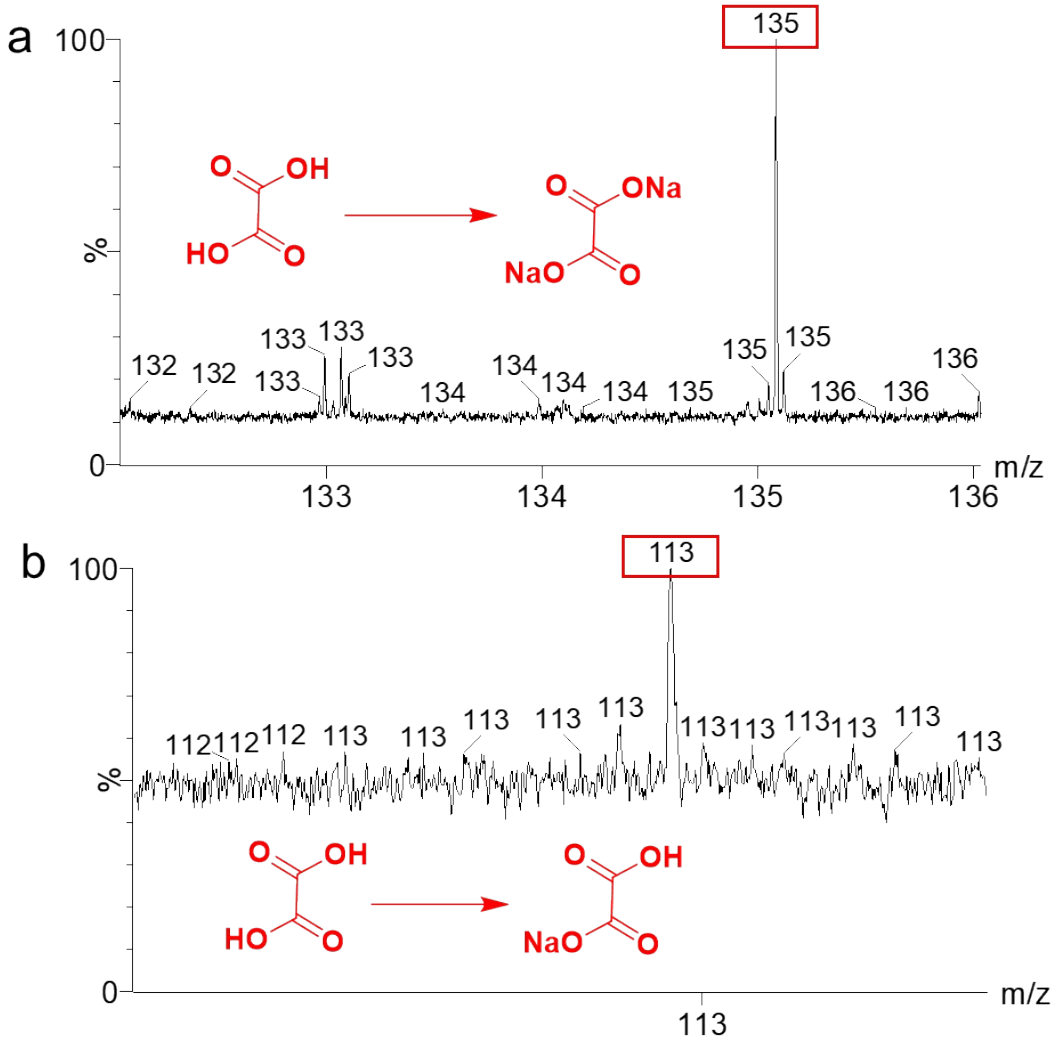

Figure S43. Mass spectrometric analysis of degradation intermediates with the identification of the maleic acid. oxalic acid.

19. Water contact angle images

To investigate the hydrophobic properties of the material as indirect evidence of the catalyst's stability, water contact angle measurements were performed[23]. The sample preparation procedure was as follows: 10 mg of OFN cocrystal powder was dispersed in a solvent system consisting of 3 mL of ultrapure water and 1 mL of anhydrous ethanol. The mixture was ultrasonicated at 100 Hz for 2 minutes to form a uniformly dispersed suspension. A Si/SiO_2 substrate was used, which had been sequentially cleaned *via* ultrasonic treatment with ultrapure water, anhydrous methanol, acetone, and isopropanol, followed by nitrogen drying. The powder particles were controllably deposited onto the substrate surface using a vertical dip-coating method. The samples were then air-dried at room temperature to ensure complete solvent removal. Finally, the contact angle was measured using a contact angle goniometer.

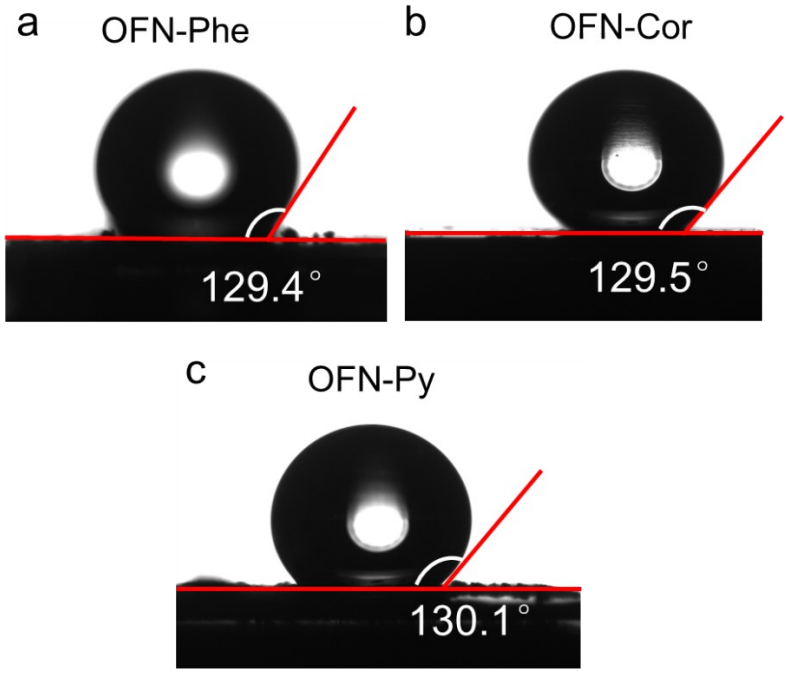

Figure S44. Water contact angle images. (a) OFN-Phe, (b) OFN-Cor and (c) OFN-Py.

20. Thermogravimetric analysis (TGA)

To investigate the thermal stability of the cocrystal systems, thermogravimetric analysis (TGA) was performed on the cocrystal powder samples using a TG 209 F3 Tarsus instrument at the AIE Institute of Tianjin University. The experiments were conducted under a nitrogen atmosphere with a flow rate of 20 mL/min, and the heating rate was set to 10 °C/min[24]. According to the thermogravimetric curves obtained (as shown in Figure S39), the sublimation temperatures of the cocrystals can be clearly identified: OFN-Phe sublimates at 136 °C, while both OFN-Py and OFN-Cor exhibit sublimation temperatures of 165 °C. These results provide a valuable basis for evaluating the thermal stability of the different cocrystal systems.

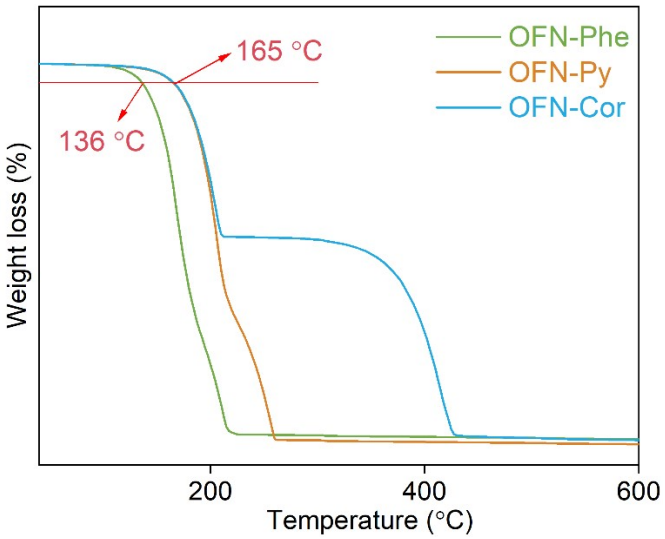

Figure S45. TGA curves of OFN-Phe, OFN-Py and OFN-Cor.

21. Theoretical Calculations

Table S5. Excitation energies of the first CT^1/CT^3/CS states of D-A dimers calculated using TD-DFT.

		Excitation energy (eV)		
		CT^1	CT^3	CS
Stacking	OFN-Cor	3.53 (S_2)	3.50	3.53 (S_2)
	OFN-Phe	4.26 (S_1)	4.34	4.50 (S_6)
	OFN-Py	3.70 (S_1)	3.70	3.70 (S_1)
Parallel misalignment along *ob*	OFN-Cor	3.36 (S_4)	3.36	3.36 (S_4)
	OFN-Phe	3.99 (S_5)	3.99	3.99 (S_5)
	OFN-Py	3.43 (S_3)	3.43	3.43 (S_3)
Parallel misalignment along *oc*	OFN-Cor	3.34 (S_4)	3.34	3.34 (S_4)
	OFN-Phe	3.99 (S_5)	3.99	3.99 (S_5)
	OFN-Py	3.44 (S_3)	3.44	3.44 (S_3)

Table S6. Hole and electron transfer couplings calculated using CDFT-CI.

Configurations	V_{HT} (eV)	V_{ET} (eV)
OFN_Cor/Cor_Cor_oa	0.000	0.001
OFN_Cor/Cor_Cor_ob	0.011	0.016
OFN_Phe/Phe_Phe_oc	0.006	0.001
OFN_Py/Py_Py_ob	0.006	0.003
OFN_Py/Py_Py_oc	0.010	0.019
OFN_Cor/OFN_Cor_oa	0.052	0.033
OFN_Cor/OFN_Cor_ob	0.055	0.035
OFN_Cor/OFN_Cor_oc	0.000	0.173
OFN_Phe/OFN_Phe_oa	0.020	0.058
OFN_Phe/OFN_Phe_ob_1	0.038	0.033
OFN_Phe/OFN_Phe_ob_2	0.000	0.001
OFN_Phe/OFN_Phe_oc_1	0.015	0.013
OFN_Phe/OFN_Phe_oc_2	0.000	0.001
OFN_Py/OFN_Py_oa	0.026	0.033
OFN_Py/OFN_Py_ob	0.001	0.001
OFN_Py/OFN_Py_obc	0.000	0.002
OFN_Py/OFN_Py_oc	0.002	0.001
OFN_Cor/OFN_OFN_oa	0.006	0.002
OFN_Cor/OFN_OFN_ob	0.007	0.006
OFN_Phe/OFN_OFN_oc	0.003	0.002
OFN_Py/OFN_OFN_ob	0.001	0.001
OFN_Py/OFN_OFN_oc	0.001	0.001

References

1. O. V. Dolomanov, L. J. Bourhis, R. J. Gildea, J. a. K. Howard and H. Puschmann, *J. Appl. Crystallogr.*, 2009, **42**, 339-341.
2. Y. Zhang, H. Wu, Y. Wang, L. Sun, S. Li, Y. Ren, Y. Sun, F. Yang, X. Zhang and W. Hu, *J. Mater. Chem. C*, 2022, **10**, 2562-2568.
3. R. A. Salinas, S. E. Martinez Tolibia, P. G. Zayas-Bazan, S. E. Rodil, M. T. Mathew, A. Navarrete, G. Santana and A. Dutt, *BME Front*, 2024, **5**, 0064.
4. J. Li, S. Ding, X. Ren, Q. Sun, L. Sun, L. Zheng, F. Li, W. Zhu and W. Hu, *ACS Mater. Lett.*, 2022, **4**, 1483-1492.
5. L. Wang, J. Deng, M. Jiang, C. Zhen, F. Li, S. Li, S. Bai, X. Zhang and W. Zhu, *J. Mater. Chem. A*, 2023, **11**, 11235-11244.
6. L. Wang, J. Deng, S. Bai, Y. Wu and W. Zhu, *Small*, 2024, **20**, 2406352.
7. L. Hao, F. Liu, X. Wang, L. Kang, Y. Wang, L. Wang, Z. Lin and W. Zhu, *Small*, 2024, **20**, 2308470.
8. S. Stoll and A. Schweiger, *J. Magn. Reson.*, 2006, **178**, 42-55.
9. D. Liu, J. Wang, X. Bai, R. Zong and Y. Zhu, *Adv Mater*, 2016, **28**, 7284-7290.
10. K. Zhang, J. Wang, W. Jiang, W. Yao, H. Yang and Y. Zhu, *Appl. Catal., B*, 2018, **232**, 175-181.
11. J. Wang, W. Shi, D. Liu, Z. Zhang, Y. Zhu and D. Wang, *Appl. Catal., B*, 2017, **202**, 289-297.
12. Q. Gao, J. Xu, Z. Wang and Y. Zhu, *Appl. Catal., B*, 2020, **271**.
13. Y. Sun, D. Wang and Y. Zhu, *Chem. Eng. J.*, 2022, **438**, 135667.
14. W. Che, C. Sun, Z. Wu, Y. Sun and Q. Shang, *J. Cleaner Prod.*, 2024, **453**, 142235.
15. S.-R. Kim, I. Ali and J.-O. Kim, *Appl. Surf. Sci.*, 2019, **477**, 71-78.
16. C. Adán, J. Carbajo, A. Bahamonde and A. Martínez-Arias, *Catal. Today*, 2009, **143**, 247-252.
17. K. Liu, L. Wang, S. Li, H. Liu, D. Zhang, M. Jiang, W. Chen, F. Jiao, X. Zhang and W. Hu, *Adv. Funct. Mater.*, 2023, **33**, 2306871.
18. A. Mandal, A. Choudhury, P. K. Iyer and P. Mal, *J. Phys. Chem. C*, 2019, **123**, 18198-18206.
19. Y. Liu, Y. Zhu, J. Xu, X. Bai, R. Zong and Y. Zhu, *Appl. Catal., B*, 2013, **142-143**, 561-567.
20. H. Xu, X. Sun, H. Yang, J. Cui, J. Wang, Y. Kang, J. Deng and G. Huang, *J. Cleaner Prod.*, 2024, **436**, 140672.
21. Y. Hu, D. Li, F. Sun, Y. Weng, S. You and Y. Shao, *J. Hazard. Mater.*, 2016, **301**, 362-370.
22. I. Wysocka, E. Kowalska, K. Trzciński, M. Łapiński, G. Nowaczyk and A. Zielińska-Jurek, *Nanomaterials*, 2018, **8**, 28.
23. X. Xu, L. Meng, J. Zhang, S. Yang, C. Sun, H. Li, J. Li and Y. Zhu, *Angew. Chem. Int. Ed.*, 2024, **63**, e202308597.
24. J. Cui, J. Li, C. Sun, Z. Gu, G. Dai, Y. Tian, J. Li, J. Feng, L. Ye, Y. Yi and W. Zhu, *Adv. Opt. Mater.*, 2025, **13**, 2403275.